**Progress In Oceanography**
January 2024, Volume 220 Pages 103186 (16p.)
https://doi.org/10.1016/j.pocean.2023.103186
https://archimer.ifremer.fr/doc/00866/97771/



# Sources, Transport, and accumulation of Mercury in the northwestern Mediterranean margin sediments during the Industrial Era and influence of turbiditic events

Cossa Daniel [1, 2, *], Buscail Roselyne [3], Dennielou Bernard [4], Radakovitch Olivier [5, 6], Puig Pere [7], Khripounoff Alexis [8], Boutier Bernard [2], Berné Serge [3]

[1] Université Grenoble Alpes, Université Savoie Mont Blanc, CNRS, IRD, IFSTTAR, ISTerre, CS 40700, F-38058 Grenoble Cedex 9, France
[2] Ifremer, Biogéochimie et Ecotoxicologie, BP 21105, F-44311 Nantes Cedex 3, France
[3] Université de Perpignan Via Domitia, Cefrem, UMR 5110, F-66860 Perpignan Cedex, France
[4] Geo-Ocean, Ifremer, Université de Brest, CNRS, UMR6538, F-29280 Plouzané, France
[5] Irsn (Institut de Radioprotection et de Sûreté Nucléaire), PSE-ENV/SRTE/LRTA, F-13115 Saint-Paul-lès-Durance, France
[6] Aix Marseille Université, CNRS, IRD, INRAE, Coll France, CEREGE, Aix-en-Provence, France
[7] Institut de Ciències del Mar, ICM-CSIC, E-08003 Barcelona, Spain
[8] Ifremer, Université de Brest, CNRS, Ifremer, UMR6197 BEEP, F-29280 Plouzané, France

* Corresponding author : Daniel Cossa, email address : dcossa@ifremer.fr

**Abstract :**

Sources and pathways of the Hg accumulated in the sediments of the Gulf of Lion (GoL) and its adjacent marine areas (Northwestern Mediterranean) have been explored using sediment grab samples, sediment cores, and sediment trap samples. The main source of Hg along this margin is the Rhône River, whose suspended sediments settle mainly in the prodelta area but also along the mid-shelf, then reaching the continental rise via wave resuspension and cascading of dense shelf waters. Seaward, these riverine particles are mixed with carbonated ooze conveyed to the bottom by the biological pump. The Hg is enriched in surface sediments of the GoL with decreasing concentrations westward and seaward from the Rhône prodelta to the continental rise. Dated cores from the Rhône prodelta give access to riverine sediments deposited over the last 400 years and show that the Hg concentration time trend resembles the evolution of coal consumption in France, peaking during in the 1960s. Similar trends were observed in sediment cores collected along the GoL slope and submarine canyons along with the preservation of traces of erosion and sediment instability events. Seaward, on the continental rise, the Hg concentration distribution suggests the deposition of fine planktonic-derived material and particles episodically advected from the shelf during deep cascading pulses. Anthropogenic Hg accumulated in GoL and continental rise sediments during the Industrialized Era is ~ 150 Mg (tons), two-thirds of which are buried in the Rhône prodelta area. Significant correlations are found between Hg and organic matter in GoL sediments, but the relationships differ between areas and are disrupted by the inputs of anthropogenic Hg and by the Hg availability in the Rhône River watershed during the pre-industrial period. The HgT availability in waters appears to be the limiting factor to the Hg enrichment of the particulate organic matter. Monomethyl

mercury (MMHg), which represents on average 0.3 % of the total Hg, was positively correlated to total Hg. Their distributions suggest in situ MMHg formation and a more effective net Hg methylation for surface sediment or particles collected in traps compared with particles buried in the sedimentary column.

**Highlights:**

► Sources and pathways of the Hg accumulated in the sediments of the Gulf of Lion (GoL) and its adjacent marine areas (Northwestern Mediterranean) have been explored. ► Anthropogenic Hg accumulated in the GoL sediments during the Industrial Era is ca. 150 Mg, mainly from the Rhône River. ► In surface sediment, the Hg enrichment factor decreases from 10.7 in the Rhône prodelta to 1.5 in the continental rise. ► The chronological trend of Hg is similar to the coal consumption peaking CE 1962. ► The monomethyl mercury abundance is a function of the total Hg content with proportions decreasing with increasing sediment depth.

## 1. Introduction

Sediments of continental margins are major geochemical sinks for natural and anthropogenic mercury (Hg) (e.g., Cossa et al., 1996; Fitzgerald et al., 2007; Mason et al., 2012). On the global scale, the Hg accumulated in continental margin sediments is estimated to be ~200 Mg $a^{-1}$ which is one-third of the Hg deep sediment burial (Outridge et al., 2018). From very early on, concentration profiles in sedimentary deposits have been used to track historical Hg contamination of coastal areas. Many chronological records faithfully reflect Hg depositional fluxes during the Industrial Era and even during the entire historical period (Bothner et al., 1980; Smith and Loring, 1981; Asmund and Nielsen, 2000; Johannessen et al., 2005; Elbaz-Poulichet et al., 2011; Boutier et al., 2012; Oliveri et al., 2016). This manner of reconstructing historical Hg deposition is based on the assumption that the sediment does not undergo too extensive physical or biological mixing and that Hg is not translocated during the early diagenesis of organic matter (OM). In the coastal areas, where accumulation rates are high, these conditions are thought to be fulfilled (Gobeil and Cossa, 1993; Cossa et al., 1996; Fitzgerald et al., 2018; Cooke et al., 2020). However, a good knowledge of depositional conditions, including sedimentation rates (SRs) and biological mixing, is required to establish a realistic chronology, to sort out the anthropogenic Hg fraction from the “natural” one, and ultimately quantify the Hg accumulation over the years.

In the northwestern Mediterranean continental margin, the Gulf of Lion (GoL), comprising a large continental shelf, slope, and rise, densely incised by submarine canyons, is under the influence of natural and anthropogenic Hg inputs from atmospheric and riverine sources, especially from the Rhône River (RR), the largest river discharging in the western Mediterranean (Mermex Group, 2011; Cossa et al., 2022). The present article aims to provide the inventory of Hg accumulation, establish a chronology of the Hg deposition for the last 400 years, and identify the main sources and transport paths. Our specific objectives are (i) providing the geographical distribution of Hg concentrations in surface sediment of the various regions of the GoL, (ii) establishing the chronology of the Hg deposition in the last 400 years, (iii) identifying the main Hg sources and main transport modes, and (iv) quantifying the anthropogenic Hg accumulation in GoL sediments during the Industrial Era (post AD 1850). For that purpose, we have analyzed material collected in sediment traps, surface sediment samples, including coastal lagoons, and dated sediment cores distributed from the Rhône prodelta to

the continental rise and in submarine canyons. The interpretation of our results has benefited from the contribution of numerous studies which cover the geological context, sedimentary characteristics, and anthropogenic influences on the study area (e.g., Zuo et al., 1991, 1997; Miralles et al., 2005, 2006; Rabineau et al., 2005; Roussiez et al., 2006; Cathalot et al., 2010; Canals et al., 2013; Fanget et al., 2013; Cossa et al., 2017, 2018a; Nizou et al., 2019; Dennielou et al., 2019; Estournel et al., 2023; Durrieu de Madron et al., 2020, 2023).

## 2. Study site

The GoL is characterized by a wide shelf and a steep continental (gradients up to 10° at the upper slope to 2° at 1800 m) dissected by a network of submarine canyons down to 2000 m (Berné and Gorini, 2005; Dennielou et al., 2009) (Fig. 1). Sedimentary materials delivered to the GoL derive mainly from riverine sources (the RR and several smaller coastal rivers), but also atmospheric deposition (Cathalot et al., 2010; Marion et al., 2010; Zebracki et al., 2015; Wu et al. 2018). The RR inputs, which contribute to more than 90 % of the total river-borne particles discharging into the GoL (Bourrin et al., 2006), dominate the deposition on the shelf, upper continental slope, and canyons (Aloïsi et al., 1979; Zuo et al., 1997), whereas the contribution from the atmosphere (mostly driven by the biological pump) increases seaward, to become nowadays the dominant particle source on the lower continental slope and rise (Durrieu de Madron et al., 2000). The SRs vary within three orders of magnitude, from 0.2 mm $a^{-1}$ at the continental rise (Zuo et al., 1991) up to 60 cm $a^{-1}$ in the nearshore part of the RR mouth, called the Roustan lobe, which is the most recent prodelta of the Rhône (Charmasson et al., 1998; Touzani and Giresse, 2002; Beaudouin et al., 2005; Vella et al., 2005; Fanget et al., 2013).

Within the Roustan lobe, the RR particle transport was estimated to be ~ 9.6 $\cdot 10^6$ Mg $a^{-1}$ (Antonelli and Provansal, 2002) and the accumulation to be ~5.8 $\cdot 10^6$ Mg $a^{-1}$ (a value calculated from the accumulation rate expressed in $m^3$ $a^{-1}$ by Sabatier et al. (2006) multiplied by a mean density of 1.7), whereas the total accumulation of sediment in the GoL sediment margin is estimated to $10 \pm 4 \cdot 10^6$ Mg $a^{-1}$ (Zuo et al., 1997). These figures mean that all the RR particulate discharge settles down in our study area and that ~60% of it is deposited within 5 km of the river mouth. It has been suggested earlier that this percentage would be close to 75%, and that two-thirds of the deposited sediments are more or less resuspended depending on the water depth (Aloisi et al., 1984; Radakovitch et al., 1999; Touzani and

Giresse, 2002; Estournel et al., 2023). The intense reworking of sedimentary material was quantified by the thickness of the surface mixed layer, which is > 30 cm in the proximal prodelta (Zuo et al, 1997). The Rhône prodeltaic sediments consist of laminated organic-rich pelitic deposits, which show alternations of more- sandy and more-carbonaceous layers. In these layers, seasonal and flood signatures are recorded, with organic-rich layers characterized by high terrigenous inputs associated with pollen grains typical of the RR watershed vegetation (Beaudouin et al., 2005; Fanget et al., 2013). According to the same authors, flood events create distinct sedimentary deposits, which are superimposed to long-term trends in accumulated sediments, including climatic and man-made changes in RR (channelization, damming, reforestation, etc.).

On the GoL shelf, storms and dense shelf-water cascading events prevent long-term sediment deposition (Guillen et al., 2006; Durrieu de Madron et al., 2008; Durrieu de Madron et al., 2023). The general westward water mass circulation directs most of the export of suspended sediment towards the southwestern exit of the GoL through re-suspension and deposition cycles along the inner shelf induced by waves and an anti-clockwise circulation (Millot, 1991; Palanques et al., 2006; Durrieu de Madron et al., 2008). This results in distinct depositional and erosional zones at the annual scale (Estournel et al., 2023) and net westward transport of the sediment toward the shelf edge of the westernmost submarine canyons. A part of the sediments entering the GoL canyons forms temporary deposits in their upper/middle reaches, which trap particulate OM and associated trace elements (Buscail et al., 1997). They are periodically resuspended during intense dense shelf-water cascading events and flushed to deeper canyon reaches and further down to the continental rise, especially through the Cap de Creus (CdC) Canyon (De Geest et al., 2008; Puig et al., 2008; Palanques et al., 2012; Stabholz et al., 2013). Thus, the CdC Canyon is the largest outlet of sediment temporarily trapped on the GoL shelf, and consequently of uppermost importance for assessing the contamination transfer from the industrialized Rhône valley to the northwestern Mediterranean deep ecosystems. Nearby, the Bourcart Canyon (BC, Fig. 1) is a less active canyon infilled by sea-level fall and Last Glacial Maximum-derived sediments (Gaudin et al., 2006).

On the outer shelf, upper slope, interfluves, and the continental rise, sediments have accumulated during the last sea-level fall and ensuing stillstand. Coarse-grained bioclastic carbonates have accumulated on the outer shelf (e.g., Rabineau et al., 2005) and submarine canyon heads (Gaudin et al., 2006), fine-grained prodeltaic mud on the upper slope, and the canyon interfluves (e.g., Tesson et al., 1990), and detrital lithogenic sediments at the base of the slope (e.g., Droz et al.,

2006). Beyond about 1700 m water depth, the continental rise is mainly occupied by two large sediment bodies, the Pyreneo-Catalan Sediment Ridge and the Rhone Deep Sea Fan. They consist of heterogeneous material mainly deposited during low stands of the sea through gravitational processes (turbidites and mass transport deposits) (e.g., Droz et al., 2001). Acoustic images of the sea-floor and shallow cores show that some turbiditic activity persisted during the Holocene (last 10 ka), as well as some erosion (Dennielou et al., 2006; 2009; Lombo Tombo et al., 2015). Seaward at the canyon mouths and lobe areas, sediments are characterized by superficial heterogeneous sandy material intercalated in hemipelagic carbonate ooze, although in some regions, over-consolidated muds are present (e.g., Droz et al., 2001; Dennielou et al. 2009). These sedimentary facies are not documented in terms of anthropogenic imprints. Recent modeling of sediment transport on the GoL shelf and slope confirms the current knowledge of the pluri-annual characteristics of the shelf sediment dynamics which includes the massive storage of sediment at the RR mouth, the accretion of the mid-shelf mud belt, the sediment transfer through the CdC Canyon, and the magnitude of sediment accumulations (Estournel et al., 2023).

## 3. Methods

### *3.1. Sampling*

Twenty-one sediment cores were collected in the RR prodelta, continental shelf, CdC Canyon and BC canyons, and the continental rise (Fig. 1) using various interface- and box-corers. In addition, we used a Kullenberg piston corer to have access to longer cores. Information on sampling dates, locations, water depths, and lengths of the cores are given in Supplementary Information (Table SI.1). The cores were sliced every 0.5 or 2 cm from the surface to 100 cm, then every 4 cm down to the bottom of the cores. Subsamples were frozen (-18°C), freeze-dried, and stored under cold (+4°C) and dark conditions until analysis. Additional 196 surface sediments (0-2 cm) were collected with an Ekman grab sampler in the nearshore areas as a part of the French monitoring network database (RNO/ROCCH website) and were subjected to similar treatments before analyses.

Time series of settling particles were collected along the GoL continental rise (Stas. I and L) at 20 m above the bottom and at the head of the CdC Canyon (Sta. HD) at 30 m above the bottom (Fig. 1) using Technicap® sediment traps PPS53 and PPS3 models, respectively. The distance from the bottom was chosen to reduce the flux of particles coming from local resuspension, which could

interfere with the signal (i.e., composition) of downward particles settling through the water column. Nine samples were collected in traps I and L in spring 2008, and 25 in trap HD from autumn 2004 to spring 2005. Station coordinates, water depth, and details about the mooring are given in Supplementary Information (Table SI.2). Sediment trap cups were filled with buffered Hg-free formaldehyde; the collected material was stored at +4 °C after sieving through a 1 mm nylon mesh to retain the large swimming organisms that occasionally enter the traps during sampling. It was then precisely divided into sub-samples for subsequent analyses using a wet sample divider (WSD-10, McLane®). A subsample from each trap was freeze-dried and stored in the dark until analysis.

### *3.2. Dating and age models*

The dating of cores has been established based on $^{210}$Pb and $^{137}$Cs vertical profiles in combination with sedimentological proxies (Fanget et al., 2013). These authors also used one $^{14}$C date for the bottom of core RHS-KS57. Sedimentation rates have been calculated using both constant flux-constant sedimentation (CFCS) and constant initial concentration (CIC) models (Appleby and Oldfield, 1978) based on $^{210}$Pb activities measured according to Radakovitch and Heussner (1999). Published SR values are presented in Table SI.3 and unpublished data are detailed in SI.1, with the periods covered by each core.

### *3.3. Chemical analyses*

Total carbon ($C_t$), organic carbon ($C_{org}$), and total nitrogen ($N_t$) were determined using freeze-dried and homogenized subsamples of sediments with an elemental analyzer (Model CN 2000, LECO®) after acidification with 2 M HCl (overnight, at 50°C) for $C_{org}$ to remove carbonates (Cauwet et al., 1990). The precision (6 replicates of a sample) for $C_{org}$ and $C_t$ analyses was 2 %, and 0.3 % for $N_t$. Concentrations are expressed as the weight percent of dry sediment (% dry weight). Calcium carbonate content was calculated from mineral carbon ($C_t$- $C_{org}$) using the molecular mass ratio $CaCO_3$:C = 100:12.

Sub-samples for total Hg (HgT) determinations were freeze-dried; sediment aliquots (~50-100 mg) were weighed in Ni boats and loaded in a semi-automatic Hg analyzer (AMA-254, Altec®) according to Guédron et al. (2011). Within this instrument, the samples are first heated in a furnace at 550 $^{o}$C under an atmosphere enriched in $O_2$ and the produced elemental Hg vapor is trapped onto a gold amalgamation device. This Hg is subsequently thermally (600 °C) released from the trap as an instant pulse and quantitatively measured by atomic absorption spectrophotometry. Our analytical

precision, appraised from replicate measurements (n = 16) of the certified reference material (CRM) MESS-3, a marine sediment certified for total metal content from the National Research Council of Canada (0.091 ± 0.009 µg $g^{-1}$), was 8 %; the accuracy, expressed in terms of the recovery rate of the CRM, was 109 %, and the detection limit, defined as 3 times the standard deviation of 6 blanks, was 0.007 µg $g^{-1}$. We report the HgT concentrations in the sediment samples on a dry weight basis after correction for the salt content of the sediment approximated from the measured porosity value of each sample and the water column salinity.

Monomethyl Hg (MMHg) determinations were performed by isotopic dilution, derivatization (propylation), and gas chromatography-inductively coupled plasma mass spectrometry (GC-ICP-MS) (Monperrus et al., 2005). This method was slightly modified by Abi-Ghanem et al. (2011) for marine sediments. A known quantity of $MM^{202}Hg$ (the CRM ERM–AE670 from the European Commission) was added to the sediment aliquot (~300mg). The MMHg was extracted using 6M $HNO_3$ (Suprapur, Merck®), and propylated with 100µL of 4% solution of sodium tetrapropylborate (Galab®). The propylated MMHg was then extracted into 300 µL of iso-octane and the detection was carried out by GC-ICP-MS (GC-Focuswith X-series, Thermo Electron®). The detection limit (3 times the standard deviation of 6 blank values) was better than 15 %. The accuracy, expressed in terms of the recovery rate of the CRM IAEA-405 (5.49 ± 0.30 ng $g^{-1}$), an estuarine sediment certified for MMHg, was 104 % and the precision (6 replicates of the CRM) was 0.02 ng $g^{-1}$. Aluminum (Al) concentrations were determined by atomic absorption spectrophotometry (SpectrAA 600, Varian) after the total dissolution of the sediment with a mixture of HCl, $HNO_3$, and HF in hermetically sealed Teflon (PFA) reactors according to the protocol described by Chiffoleau et al. (2004).

### *3.4. Mercury inventories*

The calculation of the anthropogenic Hg ($Hg_{anthr}$) accumulated in the GoL sediments during the Industrial Era (i.e., post AD 1850) has been performed by summing for each core the amount of $Hg_{anthr}$ calculated in each sedimentary layer for which we obtained Hg concentrations, then by combining the results obtained for each of individual regions (proximal and distal deltas, inner and outer shelves, CdC Canyon, and continental rise). The $Hg_{anthr}$ concentrations were calculated as the difference between measured Hg (HgT) and the pre-industrial Hg concentration in the same core (Table SI.4). The areas of each region are taken from the scientific literature (Estournel et al., 2023), and the proximal prodelta area is defined by an envelope of 3 km on either side of the mouth of the

Rhône River between the isobaths 10 and 40 m, whereas the distal part by an envelope between 40 and 100m. The $Hg_{anthr}$ inventories for each core are calculated as

$$\sum_{k=0}^{n} \binom{n}{k} \rho \ [\mathrm{Hg\ anthr}] \ V \ (1-\beta)$$

with ρ the density, β the porosity, V the volume of the layer, and [$Hg_{anthr}$] the concentration of the anthropogenic (post-AD 1850) Hg in the layer, n being the number of layers in the core. Hg background is the pre-industrial Hg concentration.

## 4. Results

### *4.1. Mercury in surface sediments*

#### *4.1.1 Lagoons and inner-shelf areas*

The results presented in this section concern the surface sediment (0-2 cm) collected within the near-shore zone by depth < 50 m all along the GoL coasts from the Spanish-French border to the Cap Sicié, West of Toulon (Suppl. Info. Fig. SI.1) and consist of 196 sediment grab samples that include harbors and lagoons. The HgT concentrations ranged from low (< 0.01 µg $g^{-1}$) to very high values (up to 4.90 µg $g^{-1}$), consistent with the nature of the bottom which includes both erosion and accumulation zones, with pristine and human-impacted levels, respectively (Fig. SI.1). Seventy-five percent of the concentrations ranged from 0.01 to 0.20 µg $g^{-1}$ with a mean of 0.08 ± 0.02 µg $g^{-1}$ which is comparable with the Hg levels found in other near-shore areas of the Mediterranean (e.g., Barghigiani et al., 1996; Di Leonardo et al., 2006). The highest concentrations were found in the harbor area of Marseille.

#### *4.1.2. Rhône prodelta, shelf, slope, and continental rise*

The means of HgT concentrations of the surface sediments of the proximal and distal parts of the Rhône Prodelta, the shelf, and the continental rise ranged from 0.06 to 0.29 µg $g^{-1}$ (Table 1). These concentration levels were always higher than the levels measured at the base of the cores (data shown below) and attest to Hg enrichments. The highest mean HgT concentration was found in the Rhône prodelta region and the lowest on the shelf break and the continental rise. The sediments of the continental slope, including CdC Canyon, present intermediate values. Our results from CdC Canyon

surface sediments (Table 1) are in the range of the HgT concentration published earlier for the same canyon and in its southern open slope, i.e., 0.071 ± 0.010 µg $g^{-1}$ (Durrieu de Madron et al., 2020).

***Table 1.*** *Surface sediments (0-1 cm). Organic carbon, C/N, Ca, Al, and HgT (mean ± 1 standard deviation, number of determinations in brackets). Rhône prodelta ($RD_P$: proximal part includes ME, 62C, and Stas. 1-4; $RD_D$: distal part includes 61D, 94-21, and Sta. 5), Gulf of Lion shelf ($SH_E$: east part includes Sta. 6, PR12, PR14, PR15, and PR18, I36, 95-19, TYR12; $SH_W$: west part includes Stas. 7-16, PR2-4, PR10-11), head of the Cap de Creus Canyon (HD includes Stas. 17-23),), head of the Bourcart Canyon (STKI19), Cap de Creus Canyon (cores G and H), continental slope (KIGC25 and TYR20), and continental rise (cores I, L, and KIGC1&2).*

| Core/ Region | $C_{org}$ (% d.w.) | C/N (at. Ratio) | Ca (%) | Al (%) | HgT (µg $g^{-1}$) |
|---|---|---|---|---|---|
| Rhône prodelta | | | | | |
| $RD_P$ | 1.71 ± 0.14 (6) | 10.9 ± 0.5 (4) | 11.9 ± 2.9 (4) | 5.32 ± 0.18 (5) | 0.160 ± 0.032 (6) |
| $RD_D$ | 1.56 ± 0.37 (3) | 11.6 ± 0.6 (3) | - | 5.53 ± 0.32 (3) | 0.289 ± 0.076 (3) |
| Gulf of Lion shelf | | | | | |
| $SH_E$ | 1.06 ± 0.15 (7) | 9.9 ± 0.6 (7) | - | 5.47 ± 0.52 (8) | 0.171 ± 0.043 (8) |
| $SH_W$ | 0.89 ± 0.36 (15) | 9.0 ± 1.0 (10) | 9.3 ± 3.4 (10) | 5.37 ± 0.59 (10) | 0.075 ± 0.037 (15) |
| Head of canyons | | | | | |
| HD | 0.60 ± 0.26 (7) | 8.9 ± 1.1 (7) | 13.7 ± 3.4 (3) | 5.06 ± 1.07 (7) | 0.060 ± 0.036 (7) |
| STKI19 | - | - | - | - | 0.055 ± 0.007 (2) |
| Cap de Creus Canyon | | | | | |
| G | 0.71 ± 0.07 (2) | 9.7 ± 0.5 (2) | 10.8 ± 0.1 (2) | 6.40 ± 0.20 (2) | 0.104 ± 0.008 (2) |
| H | 0.74 ± 0.03 (2) | 9.6 ± 0.4 (2) | 11.1 ± 0.1 (2) | 6.11 ± 0.05 (2) | 0.102 ± 0.005 (2) |
| Continental slope | | | | | |
| KIGC25 | - | - | - | - | 0.062 ± 0.002 (2) |
| TYR20 | 0.69 (1) | - | - | 4.2 (1) | 0.141 ± 0.011 (3) |
| Continental rise | | | | | |
| I | 0.46 ± 0.02 (2) | 10.0 ± 0.1 (2) | 17.0 ± 1.9 (2) | 4.53 ± 0.68 (2) | 0.056 ± 0.007 (2) |
| L | 0.39 ± 0.02 (2) | 11.2 ± 1.3 (2) | 20.6 ± 0.6 (2) | 3.60 ± 0.23 (2) | 0.072 ± 0.011 (2) |

| | | | | | |
|---|---|---|---|---|---|
| KIGC2&5 | - | - | - | - | 0.058 ± 0.002 (2) |

### *4.2. Mercury in sediment traps*

The HgT concentrations of samples collected in the sediment trap at the head of CdC Canyon (Trap HD, Fig. 1; Table SI.2) varied from 0.05 to 0.11 µg $g^{-1}$. The means of HgT, Al, Ca, $C_{org}$ concentrations, and C:N atomic ratios are given in Table 2. Temporal variations of these parameters, the sand proportion, and $\delta^{13}C$ are illustrated in figure 2. From October 2004 to January 2005, HgT concentrations remained fairly constant but dropped down during March 2005, then concentrations increased to reach a level similar to the beginning of the sampling period. These variations are parallel to those of $C_{org}$ and inverse to those of Ca, the proxy for carbonates, and inverse with the sand proportion (Fig. 2). In March, the increase in coarse material, low $C_{org,}$ and high Ca concentrations suggest the input of carbonate decomposed material. On the contrary, from April 2005 to the end of May, low C/N and high $\delta^{13}C$ values indicate the input of more recent biogenic marine particles (Fig. 2). On the continental rise (traps I and L), the time series were limited to 9 samples collected in spring 2008 (from 28 March to 6 June and from 4 April to 4 July for Stas. I and L, respectively). The particles collected were carbonate and OM-rich (Table 2), which suggests a biogenic origin, consistent with the increasing marine influence on the continental rise compared to the shelf area (see section 2); this biogenic marine material has HgT average concentrations significantly higher (t-test, *$p<0.01$*) than at Sta. HD (Table 2).

***Table 2.*** *Sediment traps (moored 20 m above the bottom). Organic carbon, C/N, $\delta^{13}C$, Ca, Al, and HgT (mean ± 1 standard deviation, number of determinations in brackets). (*) The HgT mean differs from the two others (t-test, $p<0.01$).*

| | $C_{org}$ (%) | $C/N_{at}$ | Ca (%) | HgT (µg $g^{-1}$) | HgT flux (µg $m^{-2}$ $a^{-1}$) |
|---|---|---|---|---|---|
| HD | 1.46 ± 0.09 (25) | 9.3 ± 0.7 (25) | 11.1 ± 1.39 (25) | 0.089* ± 0.024 (25) | 637 |
| I | 3.43 ± 0.71 (9) | 7.4 ± 0.9 (9) | 24.8 ± 3.0 (9) | 0.123 ± 0.008 (9) | 25 |
| L | 3.46 ± 0.68 (9) | 7.8 ± 1.4 (9) | 20.8 ± 2.9 (9) | 0.120 ± 0.023 (9) | 22 |

### *4.3. Mercury in the sediment cores*

*4.3.1. Rhône prodelta (cores ME, RHS-KS22, RHS-KS57, 61C, 62C, and 94-21)*

In the RR prodelta, six cores were collected at depths from 20 m (ME) to 98 m (61C) (Fig. 1). The locations, water depth, core length, type of corer, and date of sampling are indicated in Suppl. Info. (Table SI.1). The SRs (Table SI.3) varied largely decreasing seaward from 20-60 cm $a^{-1}$ in the proximal prodelta area to 0.2-0.6 cm $a^{-1}$ at 20 km away seaward (Zuo et al., 1997; Radakovitch et al., 1999; Charmasson et al., 1998; Beaudouin et al., 2005; Fanget et al., 2013; Miralles et al., 2005). In the 32-cm long ME, the Hg concentrations are quite homogeneous ranging from 0.19 to 0.27 µg $g^{-1}$ and averaging 0.23 ± 0.03 µg $g^{-1}$ (n = 13); this core located near the mouth of the RR gave access to the sediments accumulated during the year before the collection in September 2011. The surfaces of the piston cores RHS-KS22 and RHS-KS57 were perturbed during the sampling. The former was 835 cm long and the second 770 cm (Fig. 1). Core RHS-KS22, collected in the proximal prodelta at 0.65 km South of ME, by 42 m water depth, gave access to a time window of AD 1953-2008 (Fanget et al., 2013). Core RHS-KS22 was 200 m seaward from another piston core (KTR05, 738 cm long) collected in 1992 (Cambon et al., 1997), for which an SR of 17.5 cm $a^{-1}$ gives access to sediments deposited after AD 1960 (Beaudouin et al., 2005). Based on the same assumptions and the $^{137}Cs$ distribution, the SR of core RHS-KS22 is ca. 16 cm $a^{-1}$. The HgT concentrations in core RHS-KS22 vary widely from 0.08 to 0.77 µg $g^{-1}$ averaging 0.29 ± 0.15 µg $g^{-1}$ (n = 84). The general pattern of the HgT concentration profile with depth in Core RHS-KS22 (Fig. 3a) indicates a steady increase with increasing depth, superimposed by high-frequency variations depending on the grain size distribution of the sediments. Low HgT concentrations occurred within the sandy layers especially for depths ca. 350 and 755 cm, whereas high HgT concentrations are related to high RR discharge periods (Suppl. Info., Fig. SI.2). Core RHS-KS57, collected by 79 m depth 2.3 km south of RHS-KS22, allows assessing the Hg deposition of the last four centuries (Fanget et al, 2014). The HgT concentrations in core RHS-KS57 varied widely from 0.02 to 0.79 µg $g^{-1}$ (n = 200). The HgT profile date is illustrated in Figures 3a and 4. Noteworthy is that the HgT concentrations started strongly to increase at the beginning of the $XX^{th}$ Century and peaked during the AD 1960-70 decade. In cores 61C, 62C, and 94-12, HgT concentrations vary from 0.19 to 0.75 µg $g^{-1}$ (n = 59) and also peaked during the decade AD 1960-70 (Fig. 3b).

*4.3.2. Gulf of Lion shelf (cores I36, 95-19, TYR-12, 95-21, TYR-23, 95-9A, KIGC25, TYR20)*

Six box-cores were collected along the GoL shelf, west of the RR, between Rhône prodelta and the head of the CdC Canyon (Fig. 1). HgT concentrations converged to 0.03 µg $g^{-1}$ in the deepest parts of all the cores (Fig. 5a). In the upper part of the 6 cores, the most striking feature was the higher HgT levels in cores close to the Rhône prodelta, namely cores I36, 95-19, and TYR12; they ranged between 0.15 and 0.20 µg $g^{-1}$, whereas more westward they were close to 0.10 µg $g^{-1}$. In addition, the maximum concentration values of HgT decreased steadily westward from 0.21 µg $g^{-1}$ (I36, TYR12), 0.12-0.17 µg $g^{-1}$ (95-19, 95-21), to 0.08-0.10 µg $g^{-1}$ (TYR23, 95-9A).

Located in interfluves of GoL submarine canyons, cores KIGC25 and TYR20 (Fig. 1) exhibited profiles of contrasting HgT distributions (Fig. SI.3, Suppl. Info.). HgT distribution in core KIGC25 showed a homogeneous layer from surface sediment to 10 cm averaging 0.06 ± 0.01 µg $g^{-1}$ and below a very smoothed signal decreasing down to 0.014 µg $g^{-1}$ at 70 cm. On the other hand, the distribution in the short core TYR20 exhibited a sharp decrease from 0.15 at the surface to 0.02 µg $g^{-1}$ at 12 cm depth. These patterns suggest a massive input of material in a short period for KIGC25 and a rather slow, more regular, sediment accumulation for TYR20. No age models are available from these cores and the patterns of the vertical distribution suggest very variable sedimentary conditions and sediment sources on the interfluve.

*4.3.3. Canyons (cores G and H) and continental rise (cores I, L, and KIGC2 & 5, Fig. 6)*

In the CdC Canyon sediments HgT concentrations range from 0.02 to 0.12 µg $g^{-1}$ and the two profiles were similar (Fig. 5b), with increasing concentrations at the beginning of the XIX$^{th}$ Century and maxima occurring between AD 1950 and 1980 (Fig. 5b). The surface sediments were homogenous over the upper 3.5 cm, averaging 0.11 ± 0.01 µg $g^{-1}$ in the AD 1994-2002 period. On the GoL continental rise (cores I and L), HgT concentrations ranged from 0.03 µg $g^{-1}$ at the base of the cores to 0.08 µg $g^{-1}$ at the surface (Fig. 6) and their temporal evolutions were similar during the period AD 1800–1970, showing a steady increase with time. However, in the youngest deposits, HgT concentrations diverged; they continued to increase toward the surface in Core L, whereas a sub-surface minimum appeared on the Core I profile (Fig. 6). For the most distal collected cores (KIGC2 & 5, Fig. 1), and for which no age model was available, we observed high HgT contents in the first 8 cm below the surface followed by almost constant values (0.03 µg $g^{-1}$) down to the bottom of the core (Fig. 6b).

***4.4. Monomethyl mercury***

MMHg concentrations have been determined in 7 sediments cores including those from the Rhône prodelta (RHS-KS57, 61C, 62C), the GoL shelf (I36), the CdC Canyon (H and G), and the continental rise (L). In addition, surface sediment from the GoL shelf and material collected in the sediment traps I and L were also analyzed for their MMHg content. The overall average for the 370 samples analyzed (± one standard deviation) is 0.56 ± 0.62 ng $g^{-1}$ (i.e., 0.3% of the HgT), ranging on more than two orders of magnitude from 0.01 to 3.20 ng $g^{-1}$.

## 5. Discussion

### *5.1. Tracing Hg: terrestrial* vs *marine sources and transport*

The geographical gradients of Hg concentrations highlight the sources of Hg-enriched particulate material distributed all along the GoL sediments. Recent simulation using based on a hydrosedimentary model (Estournel et al., 2023) shows the (i) massive sediment accumulation near the Rhône prodelta, (ii) the net sediment advection westward through resuspension, (iii) the accretion along the mid-shelf, and (iv) the impact of dense shelf water cascading on sediment resuspension and erosion inside the Cap de Creus Canyon (see section 2). Here we show that the Hg sedimentary distribution is consistent with the general pattern of the sediment dynamic in the GoL, and in particular with the transfer of particles from the coast towards deeper parts of the margin during dense shelf water formation events and their subsequent cascading (Durrieu de Madron et al., 2023).

#### *5.1.1. The Rhône River as the main Hg source*

The highest HgT concentrations have been measured in lagoons, in the inner shelf, harbors, and especially in the Rhône prodelta region. On the shelf, the maximum concentration values of HgT decreased steadily westward from 0.21 µg $g^{-1}$ (I36, TYR12), 0.12-0.17 µg $g^{-1}$ (95-19, 95-21), to 0.08-0.10 µg $g^{-1}$ (TYR23, 95-9A) (Fig. 1, Fig. SI.1) with significantly higher Hg in the eastern part of the shelf compared to the western part (*t*-test, $p<0.01$, Table 2). This implies that the main Hg source for the whole area is the RR, which is a sort of truism for one of the most industrialized rivers in Europe documented for its Hg contamination (Poulier et al., 2019). This marked trend likely is consistent with the increasing proportion of material from catchments of Languedoc rivers in the western part of the GoL compared to the eastern part (Révillon et al., 2011).

#### *5.1.2. Contrasting Hg accumulation on continental shelf and slope*

Low HgT values were encountered in surface sediment at the head of the canyons (HD and STKI19), in environments where resuspension and ephemeral sediment deposition prevail (Palanques et al., 2012), making unlikely long-term sedimentary accumulation, a hypothesis consistent with the conclusion by Courp and Monaco (1990). Sta. STKI19 is located in the distal domain of the head of BC (478 m), which constitutes a bypass or erosive area as fine-grained sediments are winnowed away by the strong currents (Gaudin et al., 2006). Similarly, the head of CdC Canyon contains coarse material (DeGeest et al., 2008), which is usually associated with low Hg content (i.e., Vane et al., 2020). However, a relatively high mean concentration for the continental slope sediments was found (Sta. TYR20); this HgT value is associated with a high $C_{org}$ concentration and low lithogenic content (Table 2). On continental rise stations, HgT concentrations along the continental rise are as low as the sediments at the head of the CdC Canyon with an overall mean of 0.062 ± 0.014 µg $g^{-1}$. There, low $C_{org}$, high C/N, high Ca, and low Al values of surface sediment suggest a more mineralized OM and an increasing proportion of carbonates relative to lithogenic material, which testifies to the increasing importance of biogenic material from the water column in the seaward direction.

*5.1.3. Hg transport: role of organic matter and cascading*

In the sediments trap samples collected at Stas. HD, I, and L, the relationship between Hg and OM allows us to highlight the Hg transport. The Hg *vs* $C_{org}$ relationship is well described by an asymptotic shape (Fig. 7a). This pattern reflects two different origins for the material collected (Fig. SI.4). First, particles with low $C_{org}$ (<1%) and HgT (<0.13 µg $g^{-1}$) concentrations are those of the material trapped at Sta. HD during the cascading event recorded in winter/spring 2005, which brought resuspended material (Canals et al., 2006; Puig et al., 2008; Tesi et al., 2010; Stabholz et al., 2013; Durrieu de Madron et al., 2023) mostly composed of carbonate broken shells and OM of terrigenous origin as indicated by the low $\delta^{13}C$ values (Fig. 2). In a study on the same trap material, these carbonates have been shown to be depleted in several trace elements compared to the clays (Cossa et al., 2014a); present results show that it is also the case for Hg. Secondly, for $C_{org}$ content > 1%, i.e., outside of the cascading period, HgT concentrations remained relatively stable with small variations between 0.09-0.13 µg $g^{-1}$, in association with finer material (Fig. 2). In addition, during the post-cascading spring period, more biogenic marine material, as testified by high $\delta^{13}C$ (Fig. 2), was collected in the trap with similar Hg contents to the material collected before the cascading event. This phenomenon may result from the Hg uptake in the water column by biogenic material formed in the euphotic zone which settled in the station HD trap. Furthermore, at the sediment traps moored on

the continental rise during the year 2008 (Stas. I and L), high $C_{org}$, Ca, and low C/N values indicate higher marine inputs, which come with average HgT concentrations significantly higher than at the head (Sta. HD) of the CdC Canyon (Table 2).

In summary, the biological pump seems to scavenge the Hg present in the water column and quantitatively delivers it to the traps deployed near the seafloor in deep-sea environments. Such a process has already been proposed by Gehrke et al. (2009) for Hg transport to the sediments during the mid-Pleistocene in the western Mediterranean. It can be inferred that in the lower 20-30 m water column above the bottom (the nepheloid layer) two types of particles, and their associated Hg, settle down: (i) autochthonous biogenic ones brought by vertical transfer and (ii) reworked material from the shelf advected through cascading and other near-bottom transport processes. In terms of transport, the advective Hg flux through the CdC Canyon (637 µg $m^{-2}$ $a^{-1}$) is 25 times more intense than the vertical flux on the continental rise (24 µg $m^{-2}$ $a^{-1}$) (Table 2). Indeed, at the head of the canyon, 28% of the total downward Hg flux occurred during the cascading period which occupied less than 15% of the total sampling period.

*5.1.4. Meanings of the various Hg-OM relationships*

The role of OM as an important carrier of Hg in the GoL sediments is evidenced by our results. Indeed, the overall correlation coefficient between Hg and $C_{org}$ in sediments and material from traps is significant ($R^2$ = 0.20, n= 545, *p<0.01,* Fig. 7, Fig. SI.5) as in many other aquatic environments all over the world (e.g., Clifton and Vivian, 1975; Schäfer et al., 2006; Hare et al., 2010; Sanei et al., 2014). However, the Hg:$C_{org}$ ratios stretched over more than one order of magnitude, with higher ratios during the Industrial Era than before AD 1850 and decreasing seaward (Table 3) testifying to diverse local and temporal situations. In surface sediments of the entire GoL, the correlation between HgT and $C_{org}$ is of linear type ($R^2$ = 0.54, n = 29, *p<0.01*) with a positive regression coefficient of ~$0.1 \cdot 10^{-4}$. Considering the entire sedimentary columns, the scatterplot exhibits different relationships depending on the location and period (Fig. 7b and c). Linear HgT *vs* $C_{org}$ relationships are highly significant in most of the zones, but regression coefficients largely differ from negative values to positive ones (from $-0.63 \cdot 10^{-4}$ to $+1.09 \cdot 10^{-4}$, Table 4). This diversity of relationships is explained by the fact that, despite the proven role of OM in Hg transport, the input functions of Hg and $C_{org}$ differ over time; in other words, Hg-$C_{org}$ relationships are disrupted by the time variations of anthropogenic Hg. For example, in the sediment core of Sta. 94-21, where a decrease of Hg inputs

446 was evidenced (Fig. 3b), the Hg and $C_{org}$ are inversely correlated, whereas in surface sediments
447 (SHw, HD) they are positively correlated with the highest $R^2$ (Table 4 and Fig. 7c). In Core RHS-
448 KS57 the HgT concentrations cover various ranges depending on the date of the depositions.
449 Significant relationships were observed during the periods of anthropogenic Hg inputs since AD
450 1850, namely from AD 1850 to 1897, when the increase of Hg relatively to $C_{org}$ was low (regression
451 coefficient $+0.3 \cdot 10^{-6}$, Fig. 7c), and between AD 1897 to 1962 (the peak of Hg contamination) but
452 multiplied by a factor of 5 (regression coefficient $+1.6 \cdot 10^{-6}$, Fig. 7b). Keeping the $C_{org}$ inputs
453 constant, this would imply that anthropogenic Hg contamination in the Rhône prodelta has hastened a
454 first time around AD 1850, but augmented especially at the beginning of the XX$^{th}$ Century. Before
455 the Industrial Era (prior to AD 1850), the HgT signal in the sediment was independent of the OM
456 content (Fig. 7c), in a similar way as observed in trapped material (Fig. 7a). This implies that, within
457 the narrow $C_{org}$ range (0.4-0.6%), the HgT availability in the RR waters was the limiting factor to a
458 Hg-enrichment of the OM. Still in the same core (RHS-KS57), during the anthropogenic Hg decrease
459 period (i.e., after AD 1962), there is a total decoupling of Hg and OM content (Fig. 7b), since
460 organic-rich young deposits bring with them less and less Hg-contaminated particles.

461 ***Table 3****. HgT:$C_{org}$ (mass ratios x $10^{-4}$) in sediments from various parts of the GoL. N: number of samples.*

| Area | Core | Mean ± 1 standard deviation (min-max), N |
|---|---|---|
| Rhône Prodelta | RHS-KS57-22, 94-21 (Industrial Era) | 0.351 ± 0.257 (0.082 – 1.155), 170 |
| Rhône Prodelta | RHS-KS57 (pre-industrial period) | 0.079 ± 0.014 (0.0530 –0.136), 79 |
| Shelf | 95-9A, 95-19, 95-21, TYR91 | 0.119 ± 0.106 (0.029 – 0.705), 64 |
| CdC Canyon | G & H | 0.124 ± 0.045 (0.036 – 0.189), 53 |
| Continental rise | I & L | 0.103 ± 0.032 (0.043 – 0.172), 39 |

462

463 In summary, two sources for Hg in the GoL sediments are evidenced, continental and marine.
464 The former derives from rivers and is dispersed on the shelf and transferred to depths *via* submarine
465 canyons, with some contribution of eroded material from the shelf. Active Hg transfer from the shelf
466 sediment to the deeper parts of the margin occurs during the cascading events associated with dense
467 water formation. Seaward, the particulate Hg export is associated with marine Hg inputs from
468 atmospheric deposition, scavenged by the biological pump and reaching the sediments with the
469 settling material. During these particle transport processes, in part controlled by the particulate OM

transport, Hg overcomes phase change reactions. In this regard, it is worthwhile pointing out that the material collected in the traps was Hg-enriched, with a factor of 1.5-1.9, compared to the surface sediments below, whereas similar enrichment was much higher for the $C_{org}$ (2.5-8.0). This suggests that during the intense OM mineralization in the benthic boundary layer before its burial into the sedimentary record, the Hg is not fully mobilized and that a large proportion is reabsorbed.

***Table 4***. *HgT (µg $g^{-1}$)* versus *$C_{org}$ (%) relationships in sediment cores. $RD_P$ and $RD_D$: Rhône prodelta proximal and distal parts; $SH_E$ and $SH_W$: GoL shelf eastern and western parts; HD: Head of the CdC Canyon. NS: non-significant. In surface sediments, $R^2$ is 0.54, the regression coefficient +0.1009, and the origin +0.0234 ($p<0.01$).*

| Zone | Core | Regresson coefficient (Slope) | Origin | $R^2$ | p |
|---|---|---|---|---|---|
| Rhône prodelta | | | | | |
| $RD_P$ | RHS-KS22 | - | - | 0.03 | NS |
| $RD_P$ | RHS-KS57 | +1.0852 | –0.4138 | 0.43 | <0.01 |
| $RD_D$ | 94-21 | –0.6289 | +1.4744 | 0.60 | <0.01 |
| Gulf of Lion shelf | | | | | |
| $SH_E$ | surface | –0.0974 | +0.3146 | 0.71 | <0.01 |
| $SH_W$ | surface | +0.1441 | –0.0122 | 0.88 | <0.01 |
| $SH_W$ | 95-21&9A | +0.1111 | –0.0827 | 0.37 | <0.10 |
| Cap de Creus Canyon | | | | | |
| HD | surface | +0.13334 | –0.0194 | 0.92 | <0.01 |
| Canyon | G & H | +0.2752 | –0.0897 | 0.65 | <0.01 |
| Continental rise | | | | | |
| Rise | I & L | +0.1457 | –0.0136 | 0.66 | <0.01 |

## *5.2. Chronology of Hg accumulation*

### *5.2.1. Hg chronology in the prodelta sediments and coal emissions*

Core RHS-KS57 permits a long historical record that goes back to the beginning of the XVII$^{th}$ Century. At the base of the core, HgT concentrations reach low values of ~0.030 µg g$^{-1}$ but, at this stage, nothing indicates that this level, occurring in AD 1600, is representative of the pristine level of the prodelta sediments. Rather the time trend in HgT and HgT:$C_{org}$ ratios suggest that human influence began well before the onset of the Industrial Era (insert, Fig 4a). As early as the second part of the XVII$^{th}$, Hg concentrations grew from 0.03 (AD 1650) to 0.04 µg g$^{-1}$ (AD 1850), with most of the increase between AD 1650 and AD 1700. Elbaz-Poulichet et al. (2011) already observed in a sediment core from the Pierre-Blanche Lagoon, a Hg broad peak during the XVII$^{th}$ Century, which they attributed to the expansion of gold and silver amalgamation in Europe and particularly in the South of France (Cévennes). There, many auriferous rivers were exploited as soon as the Roman period (Domergue et al., 2006). However, the Hg increase rate enhanced at the beginning of the Industrial Era and particularly ~AD 1900, then peaking during the AD 1960-70 decade followed by a rapid decline at the end of the XX$^{th}$ Century and the first decade of the XXI$^{th}$ (Fig. 4a). The Hg increase rate in core RHS-KS57 reached 25 times between AD 1850 and AD 1962 i.e., the date of the maximum, with Hg concentrations varying from 0.04 µg g$^{-1}$ to 1.02 µg g$^{-1}$; this corresponds to an increase rate of ca. 3% a$^{-1}$ (Table 5). The decrease between AD 1962 and the first decade of the XXI$^{th}$ Century was more rapid (3.6% a$^{-1}$) allowing the HgT to drop down to 0.19 µg g$^{-1}$. This overall Hg time trend resembles the evolution of coal consumption in France which started ca. AD 1830 and culminated in the sixties with two mega drops during the two world wars of the XX$^{th}$ Century (Conus and Escudier, 2006). Such time trends have already been observed for several metals in the same core, especially for Pb, tracer coal residues and coal-burning emissions, and Zn (Core RHS-KS57, Cossa et al., 2018a), and in sediment cores collected in the Rhône River (Ferrand et al., 2012). Parallel profiles between Hg and Pb were also observed in Mediterranean sediments from a lagoon nearby (85 km west) the Rhône mouth (Elbaz-Poulichet et al., 2011) to the Levantine margin of the eastern basin (Azoury et al., 2013). At this latter location, Hg and Pb contaminations were associated with the presence of polyaromatic hydrocarbons from combustion origin. These coincidences strongly suggest a common coal-burning source for Hg and Pb. Coal consumption in France started ca. AD 1820 and gradually increased to reach 60 000 Tg at the beginning of the XX$^{th}$ Century, culminating ca. 80 000 Tg in the sixties, then dropping down until the end of the Century (Suppl. Info. Fig. SI.6; Conus and Escudier, 2006). In addition, French coal consumption during the XX$^{th}$ Century crashed during the two World wars (Fig. SI.6). The HgT concentrations in the sediments of

Core RHS-KS57 follow a similar time-trend, starting to increase in the second part of the XIX$^{th}$ Century for a 100-years long period and culminating in the sixties, then decreasing progressively until the end of the XX$^{th}$ Century (Fig. 4a). Short-term variations are superimposed to this broad pattern. After the first steady increase, HgT concentrations stood between AD 1900-1920, a period which comprises the First World War, and then increased again until AD 1925, followed by a drop covering AD 1926-1943, a period which includes the Great Recession in Europe and the first part of the Second World War. Interestingly, during the First World War, while most of the French coal production crashed, the Cevennes mining (South of France), which fed the coal consumed in the entire Rhône Valley, continued to increase between 1914 and 1920 (Chancerel, 2012). This situation is more than likely the reason why the sedimentary Hg concentrations did not decrease during the period 1914-1918 in line with the evolution of coal consumption in France (Fig. 4a). The Hg evolution between AD 1930-1943 coincides with the decrease in coal consumption which has started ca AD 1930 and extended until 1943. The co-evolution between HgT and coal consumption continued until the end of the beginning of the XXI$^{th}$ Century while France was still using several Tg of imported coal mainly for energy production.

It is worthwhile pointing out that in Core RHS-KS57, Pb concentrations peak at the end of the seventies (Cossa et al., 2018a), whereas Hg peaked ten years before (Fig. 4a). In addition to coal, other sources of Pb (and Hg) exist. The various Hg *vs* Pb relationships allow sorting out these sources depending on the period (Fig. 8a). Until the beginning of the XX$^{th}$ Century Hg and Pb covaried with low regression coefficients (0.001-0.002), during the 1900-1970 period, Hg increased steeply relative to Pb (regression coefficient 0.018), then Hg decreased tremendously and Pb remained high (regression coefficient 0.006). After AD 1990, concentrations of both metals dropped down, with a regression coefficient regaining its initial value. These variations suggest that during the 1970-1990 period, a secondary source of Pb existed. Indeed, with the advent of the oil age, the Pb has been more and more used as a gasoline additive, and its emission culminated in AD 1975, then decreased to cease in AD 2000 (Suppl. Info. Fig. SI.7a). The influence of Pb emission from gasoline consumption has been recorded in the sediment cores from CdC Canyon as shown by the low values of $^{206}$Pb:$^{207}$Pb and $^{206}$Pb:$^{208}$Pb isotopic ratios (Fig. SI.7b). The reason for the shift between the maxima of Hg and Pb, therefore, resides in the multiplicity of recent Pb sources, which are illustrated in figure 8b. The low $^{206}$Pb:$^{207}$Pb ratios (<1.175) indicate the gasoline source and occur with constant Hg concentrations. $^{206}$Pb:$^{207}$Pb ranging from 1.175 to 1.190 indicate coal sources

(Fig. SI.7b) and occur with high Hg concentrations (Fig. 8). In addition, Figure 8b allows us to characterize HgT concentrations in pre-industrial Pb sediments ($^{206/207}Pb \geq 1.20$), averaging 0.035 ± 0.003 µg $g^{-1}$ (n = 33) and 0.013 ± 0.003 µg $g^{-1}$ (n = 9) for riverine and marine sources, respectively, two values that can be taken as reliable estimates of the pre-industrial Hg levels.

***Table 5.*** *Period covered by the cores and time trends observed from the HgT concentration profiles for the various cores.*

| Station | Period (AD) | Hg time trend (% $a^{-1}$) | |
|---|---|---|---|
| | | Increase | Decrease |
| Rhône Prodelta | | | |
| RHS-KS22 | 1973 – 2008 | – | 2.0 |
| RHS-KS57 | 1600 – 1850 | 0.3 | – |
| | 1850 – 1963 | 3.0 | – |
| | 1964 – 2008 | – | 3.6 |
| 61C | 1943 – 1963 | 1.2 | – |
| | 1964 – 2008 | – | 2.8 |
| 62C | 1963 – 2008 | – | 2.7 |
| 94-21 | 1943 – 1961 | 1.9 | – |
| | 1962 – 1993 | – | 2.2 |
| Gulf of Lion Shelf | | | |
| 95-19 | 1925 – 1980 | 3.0 | – |
| 95-21 | 1925 -1970 | 2.5 | – |
| Cap de Creus Canyon | | | |
| G | 1850 – 1963 | 1.0 | – |
| | 1963 – 2005 | – | 0.2 |
| H | 1850 – 1963 | 1.2 | – |
| | 1963 – 2008 | – | 0.5 |
| Continental Rise | | | |
| I | 1850 – 2005 | 0.5 | – |
| L | 1850 – 2005 | 0.4 | – |

The entire (835 cm-long) Core RHS-KS22 covers a 36-year-long period (AD 1972-2008) which corresponds to the upper 90 cm of Core RHS-KS57. In this time interval, the main trend of Hg concentrations is similar between the two cores (Fig. 3a), showing a decrease between the seventies and the time of core collections of roughly a factor of 3-5 depending on the core. This allows calculating a Hg concentration decreasing rate of ca. 2% per year since the seventies (Table 5). Noteworthy, the Hg profile in the RHS-KS57 core exhibited roughly constant concentration since the end of the nineties (Fig. 3), which may result from the mixing of the top of the sediment collected with a piston corer. A detailed examination of HgT variations in Core RHS-KS22 indicates that low Hg concentrations coincide with sandy layers (see especially depths 350 and 755 cm in Fig. SI.2). In addition, besides the sandy influence, a positive correlation between the HgT concentrations and the RR discharge, especially with the Durance tributary discharge ($R^2 = 0.44$, n= 83, $p < 0.001$) has been found using the monitoring database of the French rivers (Hydrofrance web site). This relationship suggests a possible effect of the resuspension of Hg-rich fine sediment of the RR with increasing river discharge.

*5.2.2. Repercussion in the prodelta sediments of the recent Hg decrease in the Rhône River*

The three short box-cores (94-21, 61C, and 62C) collected in the distal part of the Rhône prodelta (Fig. 1) allow documenting more accurately the Hg evolution of the second part of the $XX^{th}$ Century; the values of their SRs range from 0.45 to 0.70 cm $a^{-1}$ (Table SI.3). Thus, the period covered by the three cores starts at the end of the Second World War. Cores 94-21 and 61C showed the highest Hg concentrations in the early sixties peaking at 0.75 and 0.58 µg $g^{-1}$; the highest HgT concentration (0.69 µg $g^{-1}$) was observed at ~AD 1962) (Fig 3b). The HgT concentrations rapidly decrease consistently towards the sediment-water interface in the three cores, attaining at the sediment surface (i.e., ~2008 AD) 0.19 and 0.28 µg $g^{-1}$ in core 62C and 61C, respectively. Noteworthy, the higher HgT concentration of core 61C corresponds to a homogenous layer probably resulting from the mixing of the top 10 cm of the sediment, equivalent to ~20 years of deposition. From the three profiles (Fig. 3b), rates of Hg decrease in the last 46 years is 1.6 % per year, a similar rate as calculated for cores RHS-KS22 and RHS-KS57. If the Hg decrease continues at the same linear rate, the pre-industrial Hg level might be reached after ~20 years; however, the decrease does not seem to be linear and an exponential model would probably be more appropriate to describe the Hg time trend since soils and

sediments of the RR basin are still Hg-enriched from the anthropogenic Hg left from the deposition of the Industrial Era. In brief, the Hg concentrations measured in the sediments of the six cores collected in the Rhône prodelta exhibit a 1.6-2 % annual decrease during the last 50 years. They also show that the most recently deposited sediments (AD 2008-2011) have a similar Hg concentration range (0.13-0.27 µg $g^{-1}$) as the annual mean of Hg concentrations in the RR suspended particles collected near the river mouth (Arles), which consistently ranged from 0.1 to 0.2 µg $g^{-1}$ for the period 2011-2016 AD (Poulier et al., 2019; Delile et al., 2022), in agreement with the Hg content of recent deposits at RR mouth ($RD_P$: 0.16 ± 0.03 µg $g^{-1}$, Table 2).

*5.2.3. Hg chronology in the slope and rise sediments*

Canyon sediments receive inputs from the GoL shelf, especially during cascading events. Deep cascading phenomena play a major role in the shelf export of particulate material, including metals, as well as their redistribution in the basin by deep convection (Durrieu de Madron et al., 2023). In the CdC Canyon sediments (cores G and H), HgT concentrations start to increase at the beginning of the $XIX^{th}$ Century to culminate between AD 1950 and 1980 (Fig. 5b). The surface sediments are homogenous over the upper 3.5 cm, averaging 0.11 ± 0.01 µg $g^{-1}$ in the AD 1994-2002 period. This chronology matches that of core RHS-KS57 strongly suggesting that the CdC Canyon is the main conduit for the exportation of particles from the RR. Hg concentrations in non-dated core STKI19, collected in the BC, varied from 0.02 to 0.08 µg $g^{-1}$ with a rapid change in HgT concentrations between 29 and 30 cm (Fig. 5c). The X-ray imaging and the $^{210}Pb$ activity performed on the same core (Gaudin et al., 2006) allowed identifying a 30-cm thick structureless upper sequence and a lower sequence. The presence of Hg-contaminated sediments, associated with measurable $^{210}Pb$ activities, only in the upper sequence of the sediments supports that the distal part of the BC head is subject to the accumulation of modern sediments. In the absence of a real age model for this core, we are constrained to hypothesize that this distal part of the head of BC has received a massive input of Hg-enriched sediment, accumulated on the shelf break thru the Industrial Era during a period of dense water cascading at the shelf edge, such as those described by Gaudin et al. (2006). Our results support the conclusion of these authors that the modern sedimentary activity of BC is made of alternative phases of deposition and erosion.

The $^{210}Pb$ inventories in continental rise sediments (cores I and L) suggest that they receive most of their material from downward settling in the upper water column, but also from particles

episodically advected from the margin during deep cascading pulses (Tesi et al., 2010; Palanques et al., 2012; Puig et al., 2013; Durrieu de Madron et al., 2023). The presence of planktonic material is attested by the coarse carbonate material, including foraminifera and pteropods, in core I, and finer planktonic-derived material in core L (Cossa et al., 2014a). The chronology of Hg deposition in core I is parallel to that of core RHS-KS57 suggesting the influence of RR inputs on the continental rise through the CdC Canyon. However, the time resolution obtained for core L does not permit access to similar details, since the last 70 years are covered with only three measurements (Fig. 6a and b). Recent anthropogenic Hg inputs and bioturbation likely control the shape of the Hg concentration increase toward the sediment surface. A similar interpretation can be applied to cores KIGC2 and 5, the upper 10 cm of which consisting of carbonated biogenic mud and SRs are in the order of 0.002 cm $a^{-1}$ (Dennielou et al., 2009). Thus, we can reasonably hypothesize that the HgT enrichment in the top of these cores on the continental rise sediments is due to anthropogenic Hg accumulated in the Industrial Era (Fig. 6b) and that the Hg profiles are affected by biomixing.

### *5.3. Anthropogenic Hg: sources and quantification*

The HgT concentration distributions observed in the near-shore surface sediments (Fig. SI.1) are consistent with those of the most recent survey by Bouchoucha et al. (2018) which identifies the Marseille harbor as a highly Hg-contaminated area of the GoL coast. The surface sediment collected in the Marseille area presented elevated concentrations ranging from 0.30 to 4.90 µg $g^{-1}$, with the highest levels found in the sediments collected in front of the main outflow of the sewage of the city of Marseille. These concentration levels exceed the Environmental Assessment Criteria for Hg in the sediments (0.20 µg $g^{-1}$) of the Convention for the Protection of the Marine Environment (OSPAR), i.e., the Hg concentration in the environment below which no chronic biological effects are expected to occur in marine organisms (Webster et al., 2009). Besides this extreme value, HgT concentrations were higher than the pre-industrial levels and have to be considered Hg-enriched. They comprise lagoons under local Hg inputs, such as the Thau lagoon near which cement and coal-gas plants have been located. To provide an order of magnitude of the Hg-enrichment of surface sediments we have calculated enrichment factors ($EF = (HgT/Al)_{surf} / (HgT/Al)_{base}$). For the regions defined in the Table 1 caption, apart from lagoons and harbors, the EF values increase from 1.5-3.7 on the continental rise, to 2.3-4.7 in the CdC Canyon, 2.9-6.4 on the GoL shelf, and 6.3-10.7 in the Rhône prodelta, pointing out the RR as the main source of these Hg-enrichments. The Rhône prodelta proximal ($RD_P$)

and the distal parts ($RD_D$) can be distinguished based on their Hg mean concentrations (t-test, $p<0.01$, Table 2).

The inventories of the anthropogenic Hg accumulated during the Industrial Era ($Hg_{anthr}$) are summarized in Table 6 and totalized an average of 152 Mg. Pre-industrial backgrounds Hg concentrations, of 0.013 to 0.035 µg $g^{-1}$ depending on the zone, have been subtracted in order to only take into account the $Hg_{anthr}$ fractions (Table SI.4). Put in perspective, this total amount, equally distributed over the 150 years of the Industrial Era, gives a virtual rate of 1 Mg accumulated each year. This figure is close to the current Hg accumulated annually in the sediments of the GoL (0.9 Mg $a^{-1}$ according to Cossa et al., 2018b). On the other hand, it is 0.5% of the Hg buried annually in all the ocean margins (200 Mg $a^{-1}$ according to Outridge et al., 2018), which is huge for an area that represents less than 1‰ of the total surface of the ocean margins.

***Table 6****. Quantities of $Hg_{anthr}$ (Mg) accumulated in various parts of the sediment of the GoL and its continental rise. The calculation method is given in Material and Methods (section 3.4.) and Table SI.4.*

| Proximal prodelta | Distal prodelta | Inner shelf | Outer shelf | CdC Canyon | Continental rise | Total |
|---|---|---|---|---|---|---|
| 63 | 33 | 10-25 | 6-30 | 1 | 20 | 132-172 |

### *5.4. Methylmercury sources*

MMHg present in the surficial sediments may originate from MMHg borne with settling material. However, there are enough pieces of evidence from which it appears that the MMHg concentrations in aquatic sediments reflect the net microbiological methylation-demethylation rates within the sediment itself (e.g., Parks et al., 2013). Here, MMHg concentrations were systematically positively correlated to the HgT regardless of the location, with $R^2$ always statistically significant ($p<0.01$) varying from 0.30 to 0.94 (Fig. SI.8). Noteworthy is that the slopes of the MMHg *vs* HgT relationships were maxima with the particles from the sediment traps. Since MMHg is always less than 1 % of the HgT, HgT can be used as a proxy of the inorganic $Hg^{II}$ which constitutes the substratum for bacterial methylation. Thus, we used a model resembling Michaelis–Menten kinetics synthesizing the enzymatic methylation and demethylation reactions to explore the MMHg *vs* HgT relationship as earlier proposed (Cossa et al., 2014b). Even empirical, such fits offer the advantage of a mechanistic foundation (i.e., enzymatic processes governing Hg methylation).

$$MMHg = \frac{a \times HgT}{Km + HgT}$$

where "*a*" is the saturation MMHg concentration and "K*m*" estimates the HgT concentration, which corresponds to MMHg half-saturation. This parameter can be used as a proxy of Hg methylation efficiency, as K*m* increases, methylation efficiency decreases. It appears from data in Table 7, that net methylation efficiency is maximum for samples collected in the sediment traps or at the surface of the sediment, and one order of magnitude smaller than K*m* values calculated for sediment cores. At the same time, the magnitude of the variance of MMHg explained by the HgT (i.e., $R^2$) is smaller in these "younger" particles suggesting that for them the methylation efficiency is not primarily controlled by HgT, but more probably governed by other processes, such as microbial activity and inorganic Hg availability for methylator microorganisms (e.g., Cossa et al., 2014b). In sediment cores, K*m* varied in a smaller range from 16.7 to 43.1 µg $g^{-1}$. The highest methylation efficiencies are found in the proximal part of the Rhône prodelta, an area known for its high rates of OM mineralization driven by sulfate-reducing bacteria (e.g., Pastor et al., 2011) also known as Hg methylators. For comparison purposes, we have calculated a similar K*m* (~ 25 µg $g^{-1}$) for a 15 cm sediment core collected in the adjacent Balearic Abyssal Plain in the western Mediterranean basin. Altogether, these results suggest that Hg net methylation is less efficient for particles buried in the sedimentary record, supporting the idea that the water column is a main source for MMHg in marine environments and that, during sediment burial, demethylation seems prevailing albeit the remanence of an MMHg background at depth. Our results support the general proposition by Jonsson et al (2012): "…a combination of thermodynamic and kinetic effects of $Hg^{II}$ solid-phase dissolution and surface desorption control the $Hg^{II}$ methylation rate in sediments and cause the large observed differences in K*m*-value." This suggests that the surficial sediment, where OM is not matured, provides a medium where Hg bounds to OM are weaker than deeper in the sediment where OM sulfidization offers stronger ligands to Hg. In addition, the recently deposited sediments are MMHg-enriched in the foraging zone of meiofauna organisms, favoring by this way its biomagnification into benthic food webs.

***Table 7****. Parameters of the Michaelis-Menten relationships between MMHg and HgT. Km (µg $g^{-1}$) values were calculated for an "a" value of 0.056 µg $g^{-1}$ estimated based on more than 1400 couple values (Cossa et al., 2014b). Italics for sediment trap samples; $RD_P$ and $RD_D$: Rhône prodelta proximal and distal parts; SH: GoL shelf; CdC: Cap de Creus; Core WB was collected in the Balearic Abyssal Plain in the Western Mediterranean (Cossa et al., 2021).*

| Zone | Core/trap | K*m* | $R^2$ | p |
|---|---|---|---|---|
| $RD_P$ | RHS-KS57 | 16.7 ± 5.5 | 0.89 | <0.001 |
| $RD_D$ | 61C-62C | 31.5 ± 7.0 | 0.61 | <0.001 |
| SH | I36 | 19.3 ± 0.3 | 0.92 | <0.001 |
| SH | Surface | 4.0 ± 0.8 | 0.70 | <0.001 |
| CdC Canyon | G & H | 43.1 ± 14.9 | 0.77 | <0.001 |
| Continental rise | L | 28.4 ± 12.0 | 0.94 | <0.001 |
| Continental rise | I-L Traps | 2.4 ± 1.2 | 0.19 | <0.05 |
| Abyssal Plain | WB | 25.4 ± 15.0 | 0.34 | <0.01 |

## 6. Summary and conclusions

1. Anthropogenic Hg has been identified in the Gulf of Lion sediments. In surface sediments, the Hg-enrichment factors decrease from 10.7 in the Rhône prodelta to 1.5 in the continental rise. The Hg distribution in surface sediments clearly shows an E-W gradient. The Rhône River is pointed as the major anthropogenic Hg source for the Gulf of Lion sediments.

2. Anthropogenic Hg accumulated since the beginning of the Industrial Era is ca. 150 Mg, mainly from the Rhône River. The majority of this accumulation has occurred in the prodelta sediments (ca. 100 Mg).

3. The chronological trend of anthropogenic Hg accumulated in the Rhône prodelta sediments indicates an abrupt increase at the beginning of the Industrial Era parallel to the coal consumption in France starting in AD 1830, exhibiting a maximum ~ AD 1962, then decreasing at the end of the $XX^{th}$ Century.

4. The Cap de Creus Canyon is a focusing path and a site of (transient/ephemeral) accumulation for Hg transported from the shelf to the continental rise, especially during deep cascading events; 20 Mg of anthropogenic Hg are accumulated in the continental rise sediments. The marine water column of the Gulf of Lion is also a Hg source for the sediments; its contribution increases seaward and quite significantly in the continental rise sediments.

5. The OM is the main carrier of Hg to the sediments. Before the Industrial Era, in the riverine sediments settled in the proximal prodelta, the Hg:$C_{org}$ mass ratios averaged $0.08 \pm 0.01 \cdot 10^{-4}$, whereas in the currently settling particles collected along the continental rise, which are mostly composed of plankton, Hg:$C_{org}$ mass ratios average $0.04 \pm 0.01 \cdot 10^{-4}$. In both cases, crossed a threshold of OM, the HgT concentrations remained unchanged (~0.04 and 0.12 μg $g^{-1}$, in riverine deposited sediment of the prodelta and marine plankton collected in the sediment traps, respectively) regardless of the $C_{org}$ contents. These observations suggest that Hg-enrichment of the scavenging OM is limited by the Hg available in the water. On the contrary, in the proximal delta sediments and during the Industrial Era, the HgT and OM covary on a wide range of concentrations, with Hg:$C_{org}$ mass ratios reaching up to $1.15 \cdot 10^{-4}$ in AD 1962; since the beginning of the XXI$^{th}$ Century, the values are stabilized around $0.25 \cdot 10^{-4}$.

6. The monomethyl mercury abundance in the sediment is a function of its total Hg content but with proportions decreasing with increasing depth. Meanwhile, the settling particles trapped near the bottom and the surficial sediments present the highest net methylation efficiencies.

## Data availability

Data has been made available in Electronic Supplementary (EXCEL file "*Data_Hg_GoL_(Cossa et al., 2023)*".

## Acknowledgments

This research has been funded by HERMIONE project (www.eu-hermione.net), a collaborative project under the European Commission's Framework Seven Program (Contract N° 226354), by the ANR (Contract Nº N00014-04-1-0379), and by AEI 10.13039/501100011033 (Grant CEX2019-000928-S). Thanks are due to B. Averty who performed MMHg analyses and to F. Marco-Miralles for HgT determinations in cores KIGC and STKI. Cores TYR12, TYR20, and TYR23 have been collected during the EROS-2000 (European River Ocean System) project supported by the European Union through the Environment and Climatological and MAST Programs and grab samples and cores 94-21, 95-9A, 9519, 95-21 and I36 have been collected in the framework of the "Réseau National

d'Observation" (RNO-ROCCH) a monitoring program run by IFREMER and funded by the French Ministry for the Environment (http://www.ifremer.fr/envlit/surveillance/rno.htm).

## References


Abi-Ghanem, C., Nakhlé, K., Khalaf, G., Cossa, D., 2011. Mercury Distribution and Methylmercury Mobility in the Sediments of Three Sites on the Lebanese Coast, Eastern Mediterranean. Archiv. Environ. Cont. Toxicol. 60 (3), 394-405. Doi:10.1007/s00244-010-9555-9

Aloïsi, J.-C., Millot, C., Monaco, A., Pauc, H., 1979. Dynamique des suspensions et mécanismes sédimentologiques sur le plateau continental du Golfe du Lion. Comptes Rendus de l'Académie des Sciences 289 (13), 879–882.

Antonelli, C., Provansal, M., 2002. Vers une ré-évaluation des matières en suspension de Rhône aval par acquisition de mesures sur toute la colonne d'eau. P. 141-148. In: Proceedings of Geomorphology: From Expert Opinion to Modelling. European Center on Geomorphological Hazards, Strasbourg. Doi:10.1016/j.geomorph.2007.06.007

Appleby, P.G., Oldfield, F., 1978. The calculation of lead-210 dates assuming a constant rate of supply of unsupported $^{210}$Pb to the sediment. CATENA 5 (1), 1-8. Doi:10.1016/S0341-8162(78)80002-2

Asmund, G., Nielsen, S.P., 2000. Mercury in dated Greenland marine sediments. Sci. Total Environ. 245, 61-72. Doi:10.1016/s0048-9697(99)00433-7

Azoury, S., Tronczyński, J., Chiffoleau, J.-F., Cossa, D., Nakhle, K., Khalaf, G., 2013. Historical Records of Mercury, Lead, and Polycyclic Aromatic Hydrocarbons Depositions in a Dated Sediment Core from the Eastern Mediterranean. Environ. Sci. Technol. 47, 7101−7109. Doi:10.1021/es4005637

Barghigiani, C., Ristori, T., Lopez-Arenas, J., 1996. Mercury in marine sediment from a contaminated area of the Tyrrhenian Sea: <20 μm grain-size fraction and total sample analysis. Sci. Total Environ. 192, (1), 63-73. Doi:10.1016/0048-9697(96)05292-8

Beaudouin, C., Suc, J.-P., Cambon, G., Touzali, A., Giresse, P., Pont, D., Aloïsi, J.-C., Marsset, T., Cochonat, P., Duzer, D., Ferrier, J., 2005. Present-day rhythmic deposition in the Grand Rhone prodelta (NW Mediterranean) according to high-resolution pollen analyses. J. Cstl. Res. 21 (2), 292-306.

Berné, S., Gorini, C., 2005 The Gulf of Lions: An overview of recent studies within the French 'Margins' Programme. Mar. Petrol. Geol. 22 (6-7), 691-6-693. Doi:10.1016/j.marpetgeo.2005.04.004

Bothner, M. H., Jahnke, R. A., Peterson, M. L., Carpenter, R., 1980. Rate of mercury loss from; contaminated estuarine sediments. Geochim. Cosmochim. Acta 44, 273-285. Doi:10.1016/0016-7037(80)90137-4

Bouchoucha, M., Tomasino, C., Brach-Papa, C., 2018. Rapport de synthèse de la campagne d'évaluation de la qualité chimique des sédiments (ROCCHSED) 2016 en Méditerranée. Département d'Océanographie et Dynamique des écosystèmes, Unité Littoral. Convention Agence de l'Eau RMC-Ifremer N° 2016-0753. Rapport RST.ODE/UL/LER-PAC/18-07. Ifremer éditeur, 39pp.

Bourrin, F., Durrieu de Madron, X., Ludwig, W., 2006. Contribution to the study of coastal rivers and associated prodeltas to sediment supply in the Gulf of Lions (NW Mediterranean Sea). Vie et Milieu—Life and Environment 56 (4), 307–314.

Boutier, B., Quintin, J.-Y., Rozuel, E., Auger, D., Bretaudeau-Sanjuan, J., 2012. Retrospective study of metal contamination time trends in the French part of the Bay of Biscay. Environ. Technol. 32 (15), 1807-1815. Doi:10.1080/09593330.2011.557398

Buscail, R., Ambatsian, P., Monaco, A., Bernat, M., 1997. $^{210}$Pb, manganese, and carbon: indicators of focusing processes on the northwestern Mediterranean continental margin. Mar. Geol. 137, 271–286. Doi:10.1016/S0025-3227(96)00055-2

Cambon, G., Suc, J.-P., Aloisi, J.-C., Giresse, P., Monaco, A., Touzani, A., Duzer, D., Ferrier, J., 1997. Modern pollen deposition in the Rhone delta area (Lagoonal and marine sediments), France. Grana 36 (2), 105-113. Doi:10.1080/00173139709362596

Canals, M., Puig, P., Heussner, S., Durrieu de Madron, X., Palanques, A., Fabres, J., 2006. Flushing submarine canyons. Nature Lond. 444 (7117), 354–357. Doi:10.1038/nature05271

Canals, M., Compagny, J. B., Martin, D., Sànchez-Vidal, A., Ramirez-Llodrà, E., 2013. Integrated study of Mediterranean deep canyons: Novel results and future challenges. Progr. Oceanogr. 118, 1-27. Doi:10.1016/j.pocean.2013.09.004

Cathalot, C., Rabouille, C., Pastor, L., Deflandre, B., Viollier, E., Buscail, R., Grémare, A., Treignier, C., Pruski, A., 2010. Temporal variability of carbon recycling in coastal sediments influenced by rivers: assessing the impact of flood inputs in the Rhoˆne River prodelta. Biogeosciences 7, 1187–1205. Doi:10.5194/bg-7-1187-2010

Charmasson, S., Radakovitch, O., Arnaud, M., Bouisset, P., Pruchon, A.S., 1998. Long-core profiles of $^{137}$Cs, $^{134}$Cs, $^{60}$Co, and $^{210}$Pb in sediment near the Rhône river (Northwestern Mediterranean Sea). Estuaries 21, 367–378. Doi:10.2307/1352836

Chancerel, P., 2012. Le Marché du charbon en France pendant la Première Guerre mondiale (1914-1921). Thèse de doctorat d'histoire. Université Paris-Ouest (Ecole doctorale Economie, organisations, société). 605 pages.

Chiffoleau, J.-F., Auger, D., Boutier, B., Rozuel, E., Truquet, I., 2004. Dosage de certains métaux dans les sédiments et la matière en suspension par absorption atomique. Méthodes d'Analyses en milieu marin, Editions Ifremer, BP 70, F-29280 Plouzané (ISSN 1637–1844).

Clifton, A.P., Vivian, C.M.G., 1975. Retention of mercury from an industrial source in Swansea Bay sediments. Nature, Lond. 253, 621-622.

Conus, M.-F., Escudier, J.-L., 2006. Cycle de vie et relation capital/travail: Application à l'industrie houillère française 1720-2004. In: Territoires européens du charbon des origines aux reconversions. p.53-73; Daumalin, X., S. Daviet, P. Mioche éditeurs. Presses universitaires de Provence, Aix-en-Provence; pp. 282. Doi:10.4000/books.pup.6241

Cooke C.A., Martínez-Cortizas, A., Bindler, R., Gustin, M.S., 2020. Environmental archives of atmospheric Hg deposition – A review. Sci. Total Environ. 709, 134800. Doi:10.1016/j.scitotenv.2019.134800

Cossa, D., Coquery, M., Gobeil, C., Martin, J.-M., 1996. Mercury Fluxes at the Ocean Margins. 229-247. In: Regional and Global Cycles of Mercury: Sources, Fluxes and Mass Balances. W. Baeyens,

R. Ebinghaus and O. Vasiliev editors. NATO ASI Series 2: Environment – Vol. 21. Kluwer Academic Publishers, Dordrecht, The Netherlands. Doi:10.1007/978-94-009-1780-4

Cossa, D., Buscail, R., Puig, P., Chiffoleau, J.-F., Radakovitch, O., Jeanty, G., Heussner, S., 2014a. Origin and accumulation of trace elements in sediments of the northwestern Mediterranean margin. Chem. Geol. 380, 61-73. Doi:10.1016/j.chemgeo.2014.04.015

Cossa, D., Garnier, C., Buscail, R., Elbaz-Poulichet, F., Mikac, N., Patel-Sorrentino, N., Tessier, E., Rigaud, S., Lenoble, V., Gobeil, C., 2014b. A Michaelis-Menten type equation for describing methylmercury dependence on inorganic mercury in aquatic sediments. Biogeochemistry 119, 35-43. Doi:10.1007/s10533-013-9924-3

Cossa, D., Durrieu de Madron, X., Schäfer, J., Lanceleur, L., Guédron, S., Buscail, R., Thomas, B., Castelle, S., Naudin, J.-J., 2017. The open sea as the main source of methylmercury in the water column of the Gulf of Lions (Northwestern Mediterranean margin). Geochim. Cosmochim. Acta 199, 212-231. Doi:10.1016/j.gca.2016.11.037

Cossa, D., Fanget, A.-S., Chiffoleau, J.-F., Bassetti, M.-A., Buscail, R., Dennielou, B., Briggs, K., Arnaud, M., Guédron, S., Berné, S., 2018a. Chronology and sources of trace elements accumulation in the Rhône pro-delta sediments (Northwestern Mediterranean) during the last 400 years. Progr. Oceanogr. 163, 161-171. Doi:10.1016/j.pocean.2017.01.008

Cossa, D., Durrieu de Madron, X., Schäfer, J., Guédron, S., Marusczak, N., Castelle, S., Naudin, J.-J., 2018b. Sources and exchanges of mercury in the waters of the Northwestern Mediterranean margin. Progr. Oceanogr. 163, 172-183. Doi:10.1016/j.pocean.2017.05.002

Cossa, D., Mucci, A., Guédron, S., Coquery, M., Radakovitch, O., Escoube, R., Campillo, S., Heussner, S., 2021. Mercury accumulation in the sediment of the Western Mediterranean abyssal plain: A reliable archive of the late Holocene. Geochim. Cosmochim. Acta 309, 1-15. Doi:10.1016/j.gca.2021.06.014

Cossa, D., Knoery, J., Bănaru, D., Harmelin-Vivien, M., Sonke, J. E., Hedgecock, I. M., Bravo, A. G., Rosati, G., Canu, D., Horvat, M., Sprovieri, F., Pirrone, N., Heimbürger-Boavida, L.-E., 2022. Mediterranean Mercury Assessment 2022: An Updated Budget, Health Consequences, and Research Perspectives. Critical Review. Environ. Sci. Technol. 56, 3840-3862. Doi:10.1021/acs.est.1c03044

Courp, T., Monaco, A., 1990. Sediment dispersal and accumulation on the continental margin of the Gulf of Lions: sedimentary budget. Cont. Shelf Res. 10, 1063–1087. Doi:10.1016/0278-4343(90)90075-W

DeGeest, A.L., Mullenbach, B.L., Puig, P., Nittrouer, C.A., Drexler, T.M., Durrieu de Madron, X., Orange, D.L., 2008. Sediment accumulation in the western Gulf of Lions, France: the role of Cap de Creus Canyon in linking shelf and slope sediment dispersal systems. Cont. Shelf Res. 28 (15), 2031–2047. Doi:10.1016/j.csr.2008.02.008

Delile, H., Dendievel, A.-M., Yari, A., Masson, M., Miège, C., Mourier, B., Coquery, M., 2022. Legacy-micropollutant contamination levels in major river basins based on findings from the Rhône Sediemnts Observatory. Hydrol. Proc. 36 (2), e14511. Doi:10.1002/hyp.14511

Dennielou, B., Huchon, A., Beaudouin, C., Berné, S., 2006. Vertical grain-size variability within a turbidite levee: Autocyclicity or allocyclicity? A case study from the Rhône neofan, Gulf of Lions, Western Mediterranean. Mar. Geol. 234 (1-4), 191-213. Doi:10.1016/j.margeo.2006.09.019

Dennielou, B., Jallet, L., Sultan, N., Jouet, G., Giresse, P., Voisset, M., Berné, S., 2009. Post-glacial persistence of turbiditic activity within the Rhone deep-sea turbidite system (Gulf of Lions, Western Mediterranean): Linking the outer shelf and the basin sedimentary records. Mar. Geol. 257 (1-4), 65-86. Doi:10.1016/j.margeo.2008.10.013

Dennielou, B., Jegou, I., Droz, L., Jouet, G., Cattaneo, A., Berné, S., Aslanian, D., Loubrieu, B., Rabineau, M., Bermell, S., 2019. Major modification of sediment routing by a large Mass Transport Deposit in the Gulf of Lions (Western Mediterranean). Mar. Geol. 411, 1-20. Doi: 10.1016/j.margeo.2019.01.011

Di Leonardo, R., Tranchida, G., Bellanca, A., Neri, R., Angelone, M., Mazzola, S., 2006. Mercury levels in sediments of the central Mediterranean Sea: A 150+ year record from box-cores recovered in the Strait of Sicily. Chemosphere 65, 2366-2376. Doi:10.1016/j.chemosphere.2006.04.076

Domergue, C. Serneels, V. Cauuet, B., Pailler, J.-M., Orzechowski, S., 2006. Mines et métallurgie en Gaule à la fin de l'âge du Fer et à l'époque romaine. Colloque du Collège de France (juillet 2006). https:www.researchgate.net/publication/292398892

Droz, L., Kergoat, R., Cochonat, P., Berné, S., 2001. Recent sedimentary events in the western Gulf of Lions(Western Mediterranean). Mar. Geol. 176, 23-37. Doi:10.1016/S0025-3227(01)00147-5

Droz, L., Dos Reis, A.T., Rabineau, M., Berné, S., Bellaiche, G., 2006. Quaternary turbidite systems on the northern margins of the Balearic Basin (Western Mediterranean): a synthesis. Geo-Mar. Lett. 26, 347-359. Doi:10.1007/s00367-006-004-0

Durrieu de Madron, X., Abassi, A., Heussner, S., Monaco, A., Aloisi, J.-C., Radakovitch, O., Giresse, P., Buscail, R., Kerhervé, P., 2000. Particulate matter and organic carbon budgets for the Gulf of Lions (NW Mediterranean). Oceanol. Acta 23 (6), 717-730.

Durrieu de Madron, X., Wiberg, P., Puig, P., 2008. Sediment dynamics in the Gulf of Lions: Impact of extreme events. Cont. Shelf Res. 28 (15), 1867-1876. Doi:10.1016/j.csr.2008.08.001

Durrieu de Madron, X., Stabholz, M., Heimbürger-Boavida, L.-E., Aubert, D., Kerhervé, P., Ludwig, W., 2020. Approaches to evaluate spatial and temporal variability of deep marine sediment characteristics under the impact of dense water formation events. Mediterr. Mar. Sci. 21 (3), 527–544. Doi:10.12681/mms.22581

Durrieu de Madron, X., Aubert, D., Charrière, B., Kunesch, S., Menniti, C., Radakovitch, O., Sola, J., 2023. Impact of dense water formation on the transfer of particles and trace metals from the coast to the deep in the northwestern Mediterranean. Water, 15 (2), 301. Doi: 10.3390/w15020301

Elbaz-Poulichet, F., Dezileau, L., Freydier, R. Cossa, D., Sabatier, P., 2011. A 3500-Year Record of Hg and Pb Contamination in a Mediterranean Sedimentary Archive (The Pierre Blanche Lagoon, France). Environ. Sci. Technol. 45, 8642-8647. Doi:10.1021/es2004599

Estournel, C., Mikolajczak, G., Ulses, C., Bourrin, F., Canals, M., Charmasson, S., Doxaran, D., Duhaut, T., Durrieu de Madron, X., Marsaleix, P., Palanques, A., Puig, P., Radakovitch, O., Sanchez-Vidal, A., Verney, R., 2023. Sediment dynamics in the Gulf of Lion (NW Mediterranean Sea) during

two autumn-winter periods with contrasting meteorological conditions. Progr. Oceanogr. 210, 102042. Doi:10.1016/j.pocean.2022.102942

Fanget, S., Bassetti, M.-A., Arnaud, M. Chiffoleau, J.-F., Cossa, D., Goineau, A., Fontanier, C., Buscail, R., Jouet, G., Maillet, G.M., Negri, A., Dennielou, B., Berné, S., 2013. Historical evolution and extreme climate events during the last 400 years on the Rhone prodelta (NW Mediterranean). Mar. Geol. 346, 375-391. Doi: 10.1016/j.margeo.2012.02.007

Fanget, A.-S., Berné, S., Jouet, G., Bassetti, M.-A., Dennielou, B., Maillet, G. M., Tondut, M., 2014. Impact of relative sea level and rapid climate changes on the architecture and lithofacies of the Holocene Rhone subaqueous delta (Western Mediterranean Sea). Sediment. Geol. 305, 35–53. Doi:10.1016/j.sedgeo.2014.02.004

Ferrand, E., Eyrolle, F., Radakovitch, O., Provansal, M., Dufour, S., Vella, C., Raccasi, G., Gurriaran, R., 2012. Historical levels of heavy metals and artificial radionuclides reconstructed from overbank sediment records in lower Rhône River (South-East France). Geochim. Cosmochim. Acta 82, 163-182. Doi:10.1016/j.gca.2011.11.023

Fitzgerald, W.F., Lamborg, C.H., Hammerschmidt, C.R., 2007.Marine biogeochemical cycling of mercury. Chem. Rev. 107, 641–662. Doi:10.1021/cr050353m

Fitzgerald, W.F., Engstrom, D.R., Hammerschmidt, C.R., Lamborg, C.H., Balcom, P.H., Lima-Braun, A.L., Bothner, M.H., Reddy, C.M., 2018. Global and local sources of mercury deposition in coastal New England reconstructed from a Multiproxy, high-resolution, estuarine sediment record. Environ. Sci. Technol. 52 (14), 7614-7620. Doi:10.1021/acs.est.7b06122

Gaudin, M, Berné, S, Jouanneau, J-M, Palanques, A, Puig, P, Mulder, T, Cirac, P, Rabineau, M, Imbert, P., 2006. Massive sand beds attributed to deposition by dense water cascades in the Bourcart canyon head, Gulf of Lions (northwestern Mediterranean Sea). Mar. Geol. 234, 111-128. Doi:10.1016/j.margeo.2006.09.20

Gehrke, G.E., Blum, J.D., Meyers, P.A., 2009. The geochemical behavior and isotopic composition of Hg in a mid-Pleistocene western Mediterranean sapropel. Geochim. Cosmochim. Acta 73, 1651–1665. Doi:10.1016/j.gca.2008.12.012

Gobeil, C., Cossa, D., 1993. Mercury in the sediments and sediment pore waters in the Laurentian trough. Can. J. Fish. Aquat. Sci. 50, 1794-1800. Doi:10.1139/f93-201

Guédron, S., Cossa, D., Grimaldi, M., Charlet, L., 2011. Methylmercury in tailing ponds of Amazonian gold mines (French Guiana): Field observations and experimental flocculation method for in situ remediation. Appl. Geochem. 26, 222-229. Doi:10.1016/j.apgeochem.2010.11.022

Guillen, J., Bourrin, F., Palanques, A., Durrieu de Madron, X., Puig, P., Buscail, R., 2006. Sediment dynamics during wet and dry storm events on the Têt inner shelf (SW Gulf of Lions). Mar. Geol. 234 (1-4), 129-142. Doi:10.1016/j.margeo.2006.09.018

Hare, A.A., Stern, G.A., Kuzyk, Z.Z.A., Macdonald, R.W., Johannessen, S.C., Wang, F., 2010. Natural and Anthropogenic Mercury Distribution in Marine Sediments from Hudson Bay, Canada. Environ. Sci. Technol. 44 (15), 5805–5811. Doi:10.1021/es100724y

Hydrofrance web site. https://www.rdbrmc.com/hydroreel2/index.php

940 Johannessen, S.C., Macdonald, R.W., Eek, K.M., 2005. Historical Trends in Mercury Sedimentation
941 and Mixing in the Strait of Georgia, Canada. Environ. Sci. Technol. 39 (12), 4361–
942 4368. Doi:10.1021/es040535i

943 Jonsson, S., Skyllberg, U., Nilsson, M.B., Westlund, P.-O., Shchukarev, A., Lundberg, E., Björn, E.,
944 2012. Mercury Methylation Rates for Geochemically Relevant HgII Species in Sediments. Environ.
945 Sci. Technol. 46, 11653-11659. Doi:10.1021/es3015327

946 Lombo Tombo, S., Dennielou, B., Berne, S., Bassetti, M.-A., Toucanne, S., Jorry, S., Jouet, G.,
947 Fontanier, C., 2015. Sea-level control on turbidite activity in the Rhone canyon and the upper fan
948 during the Last Glacial Maximum and Early deglacial. Sed. Geol. 323, 148-166.
949 Doi:10.1016/j.sedgeo.2015.04.009

950 Marion, C., Dufois, F., Arnaud, M., Vella, C., 2010. In situ record of sedimentary processes near the
951 Rhône River mouth during winter events (Gulf of Lions, Mediterranean Sea). Cont. Shelf Res. 30 (9),
952 1095-1107. Doi:10.1016/j.csr.2010.02.015

953 Mason, R.P., Choi, A.L., Fitzgerald, W.F., Hammerschmidt, C.R., Lamborg, C.H., Soerensen, A.L.,
954 Sunderland, E.M., 2012. Mercury biogeochemical cycling in the ocean and policy implications.
955 Environ. Res. 119, 101-117. Doi :10.1016/j.envres.2012.03.013

956 Mermex Group (Durrieu de Madron, X., Guieu, C., Sempéré, R., Conan, P., Cossa, D. et al.), 2011.
957 Marine ecosystems' responses to climatic and anthropogenic forcings in the Mediterranean. Progr.
958 Oceanogr. 91, 97-166. Doi:10.1016/j.ocean.2011.02.003

959 Millot, C., 1991. Mesoscale and seasonal variabilities of the circulation in the Western
960 Mediterranean. Dyn. Atm. Oceans 15, 179–214. Doi:10.1016/0377-0265(91)90020-G

961 Miralles, J., Radakovitch, O., Aloïsi, J.-C., 2005. $^{210}$Pb sedimentation rates from the Northwestern
962 Mediterranean margin. Mar.Geol. 216, 155–167. Doi:10.1016/j.margeo.2005.02.020

963 Miralles, J., Véron, A.J., Radakovitch, O., Deschamps, P., Tremblay, T., Hamelin, B., 2006.
964 Atmospheric lead fallout over the last century recorded in Gulf of Lions sediments (Mediterranean
965 Sea). Mar. Pollut. Bull. 52, 1364-1371. Doi:10.1016/j.marpolbul.2006.03.018

966 Monperrus, M., Tessier, E., Amouroux, D., Leynaert, A., Huonnic, P., Donard, O.F.X., 2005.
967 Mercury methylation, demethylation and reduction rates in coastal and marine surface waters of the
968 Mediterranean Sea. Mar. Chem. 107 (1), 49-63. Doi:10.1016/j.marchem.2007.01.018

969 Nizou, J., Dennielou, B., Révillon, S., Bassetti, M. A., Jouet, G., Berné, S., Nonnotte, P., Liorzou, C.,
970 2019. Records of Holocene climatic fluctuations and anthropogenic lead input in elemental
971 distribution and radiogenic isotopes (Nd and Pb) in sediments of the Gulf of Lions (Southern
972 France). The Holocene 29 (8), 1292-1304. Doi:10.1177/0959683619846973

973 Oliveri, E., Salvagio Manta, D., Bonsignore, M., Cappello, S., Tranchida, G., Bagnato, E., Sabatino,
974 N., Santisi, S., Sprovieri, M., 2016. Mobility of mercury in contaminated marine sediments:
975 Biogeochemical pathways. Mar. Chem. 186, 1-10. Doi:10.1016/j.marchem.2016.07.002

976 Outridge, P.M., Mason, R.P., Wang, F., Guerrero, S., Heimbüger-Boavida, L.-E., 2018. Updated
977 global and oceanic mercury budgets for the United Nations Global Mercury Assessment 2018.
978 Environ. Sci. Technol. 52, 11466–11477. Doi:10.1021/acs.est.8b01246

979 Palanques, A., Durrieu de Madron, X., Puig, P., Fabres, J., Guillen, J., Calafat, A., Canals, M.,
980 Heussner, S., Bonnin, J., 2006. Suspended sediment fluxes and transport processes in the Gulf of

Lions submarine canyons. The role of storms and dense water cascading. Mar. Geol. 234, 43–61. Doi:10.1016/j.margeo.2006.09.002

Palanques, A., Puig, P., Durrieu de Madron, X., Sanchez-Vidal, A., Pasqual, C., Martín, J., Calafat, A., Heussner, S., Canals, M., 2012 Sediment transport to the deep canyons and open-slope of the western Gulf of Lions during the 2006 intense cascading and open-sea convection period. Progr. Oceanogr. 106, 1-15. Doi:10.1016/j.pocean.2012.05.002

Parks, J.M., Johs, A., Podar, M., Bridou, R., Hurt Jr., R.A., Smith, S.D., Tomanicek, S.J., Qian, Y., Brown, S.D., Brandt, C.C., Palumbo, A.V., Smith, J.C., Wall, J.D., Elias, D.A., Liang, L., 2013. The genetic basis for bacterial mercury methylation. Science 339 (6125), 1332–1335. Doi:10.1126/science.1230667

Pastor, L., Cathalot, C., Deflandre, B., Viollier, E., Soetaert, K., Meysman, F.J.R., Ulses, C., Metzger, E., Rabouille, C., 2011. Modeling biogeochemical processes in sediments from the Rhone River prodelta area (NW Mediterranean Sea). Biogeosciences 8, 1351-1366. Doi:10.5194/bg-8-1351-2011

Poulier, G., Launay, M., Le Bescond, C., Thollet, F., Coquery, M., Le Coz, J., 2019. Combining flux monitoring and data reconstruction to establish annual budgets of suspended particulate matter, mercury, and PCB in the Rhône River from Lake Geneva to the Mediterranean Sea. Sci. Total Environ. 658, 457-473. Doi:10.1016/j.scitotenv.2018.12.075

Puig, P., Palanques, A., Orange, D.L., Lastras, G., Canals, M., 2008. Dense shelf water cascades and sedimentary furrow formation in the Cap de Creus Canyon, northwestern Mediterranean Sea. Cont. Shelf Res. 28 (15), 2017– 2030. Doi:10.1016/j.csr.2008.05.002

Puig, P., Durrieu de Madron, X., Salat, J., Schroeder, K., Martín, J., Karageorgis, P. A., Palanques, A. Roullier, F., Lopez-Jurado, J. L., Emelianov, M., Moutin, T., Houpert, L., 2013. Thick bottom nepheloid layers in the western Mediterranean generated by deep dense shelf water cascading. Progr. Oceanogr. 111, 1-23. Doi:10.00310.1016/j.pocean.2012.10.003

Radakovitch, O., Charmasson, S., Arnaud, M., Bouisset, P., 1999. $^{210}$Pb and Caesium Accumulation in the Rhône Delta Sediments. Est. Ctl. Shelf Sci. 48, 77–92. Doi:10.1006/ecss.1998.0405

Radakovitch, O., Heussner, S., 1999. Fluxes and budget of $^{210}$Pb on the continental margin of the Bay of Biscay (northeastern Atlantic). Deep Sea Res. Part II 46 (10), 2175-2203. Doi:10.1016/S0967-0645(99)00059-4

Rabineau, M., Berné, S., Aslanian, D., Olivet, J.-L., Joseph, P., Guillocheau, F., Bourillet, J.-F., Ledrezen, E., Granjeon, D., 2005. Sedimentary sequences in the Gulf of Lion: A record of 100,000 years climatic cycles. Mar. Petrol. Geol. 22 (6-7), 775-804. Doi:10.1016/j.marpetgeo.2005.03.010

Révillon, S., Jouet, G., Bayon, G., Rabineau, M., Dennielou, B., Hémond, C., Berné, S., 2011. The provenance of sediments in the Gulf of Lions, western Mediterranean Sea. Geochem. Geophys. Geosyst. 12, Q08006. Doi:10.1029/2011GC003523

RNO/ROCCH. https://wwz.ifremer.fr/littoral/Reseaux-de-surveillance/Environnement/ROCCH-Reseau-d-Observation-de-la-Contamination-CHimique-du-littoral.

RNO. 1998. Surveillance du Milieu Marin. Travaux du RNO. Edition 1998. Ifremer et Ministère de l'Aménagement du Territoire et de l'Environnement. https://archimer.ifremer/doc/00314/42561. http://envlit.ifremer.fr/content/download/27652/224839/version/2/file/rno98.pdf

Roussiez, V., Ludwig W., Monaco A., Probst J.-L, Bouloubassi I., Buscail R., Saragoni, G., 2006. Sources and sinks of sediment-bound contaminants in the Gulf of Lions (NW Mediterranean Sea): a multi-tracer approach. Cont. Shelf Res. 26 (16), 1843–1857. Doi:10.1016/j.csr.2006.04.010

Sabatier, F., Maillet, G., Provansal, M., Fleury, T.-J., Suanez, S., Vella, C., 2006. Sediment budget of the Rhone delta shoreface since the middle of the 19th century. Mar. Geol. 234, 143–157. Doi:10.1016/j.margeo.2006.09.022

Sanei, H., Outridge, P.M., Stern, G.A., Macdonald R.W., 2014. Classification of mercury–labile organic matter relationships in lake sediments. Chem. Geol. 373, 87-92. Doi:10.1016/j.chemgeo.2014.02.029

Schäfer, J., Blanc, G., Audry, S., Cossa, D., Bossy, C., 2006. Mercury in the Lot-Garonne River system (France): sources, fluxes, and anthropogenic component. Appl. Geochem. 21, 515e527. Doi:10.1016/j.apgeochem.2005.12.004

Stabholz, M., Durrieu de Madron, X., Canals, M., Khripounoff, A., Taupier-Letage, I., Testor, P., Heussner, S., Kerhervé, P., Delsaut, N., Houpert, L., Lastras, G., Dennielou, B., 2013. Impact of open-ocean convection on particle fluxes and sediment dynamics in the deep margin of the Gulf of Lions. Biogeosciences 10, 1097–1116. Doi:10.5194/bg-10-1097-2013

Smith, J.N., Loring, D.H., 1981. Geochronology for mercury pollution in the sediments of the Saguenay Fjord, Quebec. Environ. Sci. Technol. 15 (8), 944-951. Doi:10.1021/es00090a010

Tesi, T., Puig, P., Palanques, A, Goñi, M.A., 2010. Lateral advection of organic matter in cascading-dominated submarine canyons. Progr. Oceanogr. 84, 185-203. Doi:10.1016/j.pocean.2009.10.004

Tesson, M., Gensous, B., Allen, G., Ravenne, C., 1990. Late Quaternary Lowstand Wedges on the Rhône Continental Shelf, France. Mar. Geol. 91 (4), 325-332. Doi:10.1016/0025-3227(90)90053-M

Touzani, A., Giresse, P., 2002. The Rhône River Prodelta: Short-Term ($10^0$-$10^3$ Year) Sedimentation Patterns and Human Impact. J. Cstl. Res. 18 (1), 102-117. West Palm Beach (Florida), ISSN0749-0208.

Vane, C.H., Kim, A.W., Emmings, J., Turner, G.H., Moss-Hayes, V., Lort, J.A., Williams, P.J., 2020. Grain size and organic carbon controls polyaromatic hydrocarbons (PAH), mercury (Hg), and toxicity of surface sediments in the River Conwy Estuary, Wales, UK. Mar. Pollut. Bull. 158, 11412. Doi:10.1016/j.marpolbul.2020.111412

Vella, C., Fleury, T.-J., Raccasi, G., Provansal, M., Sabatier, F., Bourcier, M., 2005. Evolution of the Rhône delta plain in the Holocene. Mar. Geol. 222-223, 235-265. Doi:10.1016/j.margeo.2005.06.028

Webster, L., Fryer, R., Davies, I., Roose, P., Moffat, C., 2009. Background Document on CEMP Assessment Criteria for QSR 2010. Monitoring and Assessment Series. OSPAR Commission. Publication Number: 461/2009. https://www.ospar.org/documents?v=7167

Wu, J., Rabouille, C., Charmasson, S., Reyss, J.-L., Cagnat, X., 2018. Constraining the origin of recently deposited particles using natural radionuclides $^{7}$Be and $^{234}Th_{ex}$ in deltaic sediments Cont. Shelf Res. 165, 106-119. Doi:10.1016/j.csr.2018.06.010

Zebracki, M., Eyrolle-Boyer, F., Evrard, O., Claval, D., Mourier, B., Gairoard, S., Cagnat, X., Antonelli, C., 2015 Tracing the origin of suspended sediment in a large Mediterranean river by combining continuous river monitoring and measurement of artificial and natural radionuclides. Sci. Total Environ. 502, 122-132. Doi:10.1016/j.scitotenv.2014.08.082

Zuo, Z., Eisma, D., Berger, G.W., 1991. Determination of sediment accumulation and mixing rates in the Gulf of Lions, Mediterranean Sea. Oceanol. Acta 14 (3), 253-262. https://archimer.ifremer.fr 0399-1784/91/03 253

Zuo, Z., Eisma, D., Gielest, R., Beks, J., 1997. Accumulation rates and sediment deposition in the northwestern Mediterranean. Deep-Sea Res. Part II 44 (34), 591409. Doi:10.1016/S0967-0645(96)00083-5

# Table captions

**Table 1.** Surface sediments (0-1 cm). Organic carbon, C/N, Ca, Al, and HgT (mean ± 1 standard deviation, number of determinations in brackets). Rhône prodelta ($RD_P$: proximal part includes ME, 62C, and Stas. 1-4; $RD_D$: distal part includes 61D, 94-21, and Sta. 5), Gulf of Lion shelf ($SH_E$: east part includes Sta. 6, PR12, PR14, PR15, and PR18, I36, 95-19, TYR12; $SH_W$: west part includes Stas. 7-16, PR2-4, PR10-11), head of the Cap de Creus Canyon (HD includes Stas. 17-23),), head of the Bourcart Canyon (STKI19), Cap de Creus Canyon (cores G and H), continental slope (KIGC25 and TYR20), and continental rise (cores I, L, and KIGC1&2).

**Table 2.** Sediment traps (moored 20 m above the bottom). Organic carbon, C/N, $\delta^{13}C$, Ca, Al, and HgT (mean ± 1 standard deviation, number of determinations in brackets). (*) The HgT mean differs from the two others (t-test, *$p<0.01$*).

**Table 3**. HgT:$C_{org}$ (mass ratios x $10^{-4}$) in sediments from various parts of the GoL. N: number of samples.

**Table 4**. HgT (µg $g^{-1}$) *versus* $C_{org}$ (%) relationships in sediment cores. $RD_P$ and $RD_D$: Rhône prodelta proximal and distal parts; $SH_E$ and $SH_W$: GoL shelf eastern and western parts; HD: Head of the CdC Canyon. NS: non-significant. In surface sediments, $R^2$ is 0.54, the regression coefficient +0.101, and the origin +0.023 *($p<0.01$)*.

**Table 5.** Period covered by the cores and time trends observed from the HgT concentration profiles (↑ increase, ↓ decrease) for the various cores.

**Table 6**. Quantities of $Hg_{anthr}$ (Mg) accumulated in various parts of the sediment of the GoL and its continental rise. The calculation method is given in Material and Methods (section 3.4.) and Table SI.4.

**Table 7**. Parameters of the Michaelis-Menten relationships between MMHg and HgT. K*m* (µg $g^{-1}$) values were calculated for an "*a*" value of 0.056 µg $g^{-1}$ estimated based on more than 1400 couple values (Cossa et al., 2014). Italics for sediment trap samples; $RD_P$ and $RD_D$: Rhône prodelta proximal and distal parts; SH: GoL shelf; CdC: Cap de Creus; Core WB was collected in the Balearic Abyssal Plain in the Western Mediterranean (Cossa et al., 2021).

## Figure captions

**Figure 1.** Sample sites in the Gulf of Lion (GoL). CdC: Cap de Creus; BC: Bourcart Canyon; Open circles: grab samples; filled circles: sediment cores; Red cross: sediment traps. The brown line indicates the limit of the continental shelf (isobath 200 m); the blue lines indicate the axes of the canyons.

**Figure 2.** Mercury (HgT) concentrations and chemical characteristics of the material collected in trap HD located at the head of Cap de Creus Canyon during the period October 2004 - June 2005.

**Figure 3**. Mercury (HgT) concentration profiles *versus* time in the sediment cores collected Rhône prodelta area. (a) cores RHS-KS22 and RHS-KS57; (b) cores 61C, 62C, and 94-21.

**Figure 4**. (a) Mercury (HgT), (b) organic carbon ($C_{org}$), and (c) aluminum (Al) concentration profiles *versus* time in the sediment cores RHS-KS57 collected Rhône prodelta area. The insert is an enlarged scale for HgT and HgT:$C_{org}$ ratio. WWI and WWII refer to World War I and II, respectively.

**Figure 5**. Mercury (HgT) concentration profiles *versus* time or depth in the sediment cores from the shelf (a), the CdC Canyon (b), and BC Canyon (c).

**Figure 6**. Mercury (HgT) concentration profiles in the sediment cores from the continental rise. (a) cores I and L *versus* time and (b) cores I, L, KIGC2, and KIGC5 *versus* depth.

**Figure 7**. Mercury (HgT) concentrations *versus* organic carbon ($C_{org}$). (a) the entire data set, and (b and c) for particular periods and core locations. (SHw) west part of the shelf, (HD) head of the CdC Canyon. Since HgT is expressed as µg $g^{-1}$ and $C_{org}$ as %, the regression coefficient in mass should be multiplied by $10^{-4}$.

**Figure 8**. Mercury (HgT) concentrations *versus* lead (Pb) concentrations according to various periods in core RHS-KS57. (a) HgT *versus* Pb; (b) HgT *versus* stable isotope Pb ratios.

# Figures

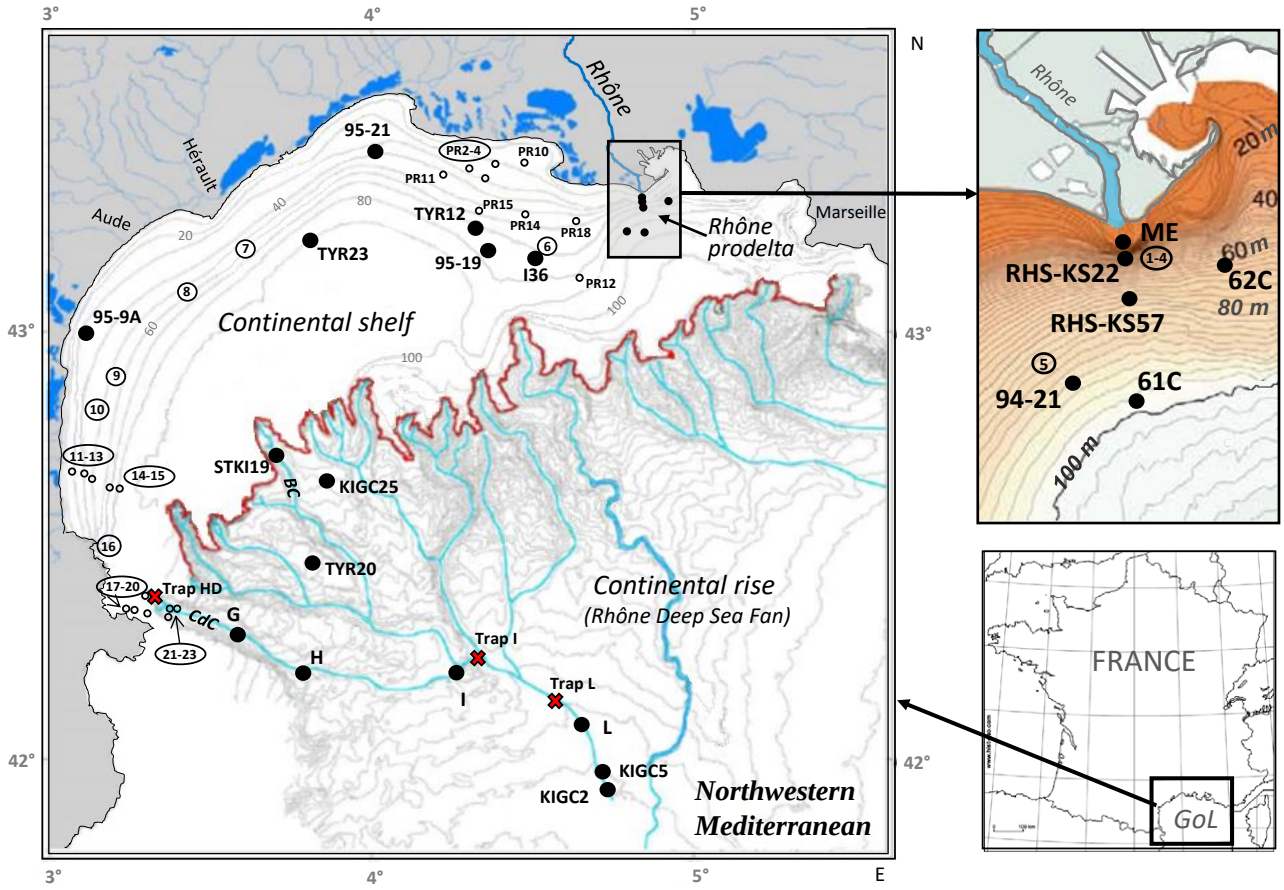


**Figure 1.**

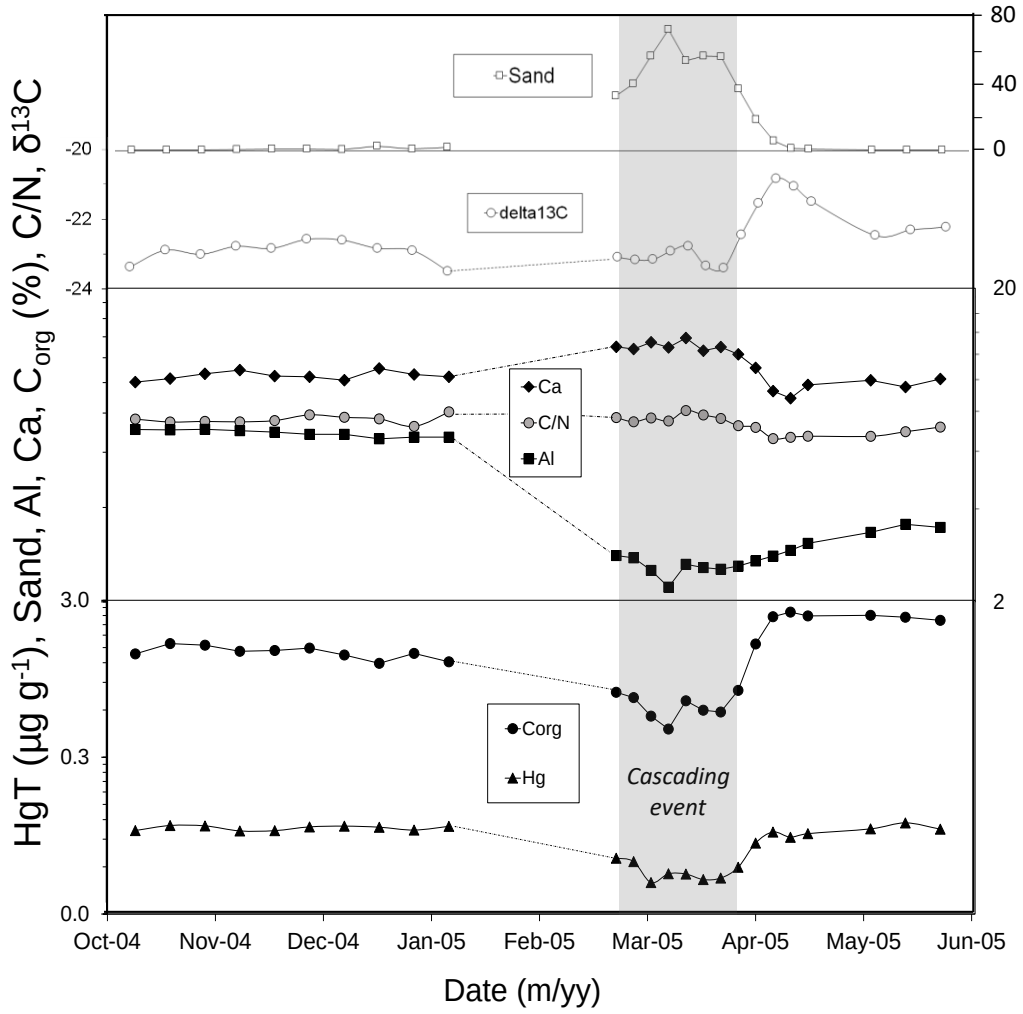
Sand
delta13C
Ca
C/N
Al
Corg
Hg
Cascading event
HgT (µg g-1), Sand, Al, Ca, Corg (%), C/N, δ13C
Date (m/yy)
Oct-04
Nov-04
Dec-04
Jan-05
Feb-05
Mar-05
Apr-05
May-05
Jun-05
80
40
0
20
2
-20
-22
-24
3.0
0.3
0.0

**Figure 2.**

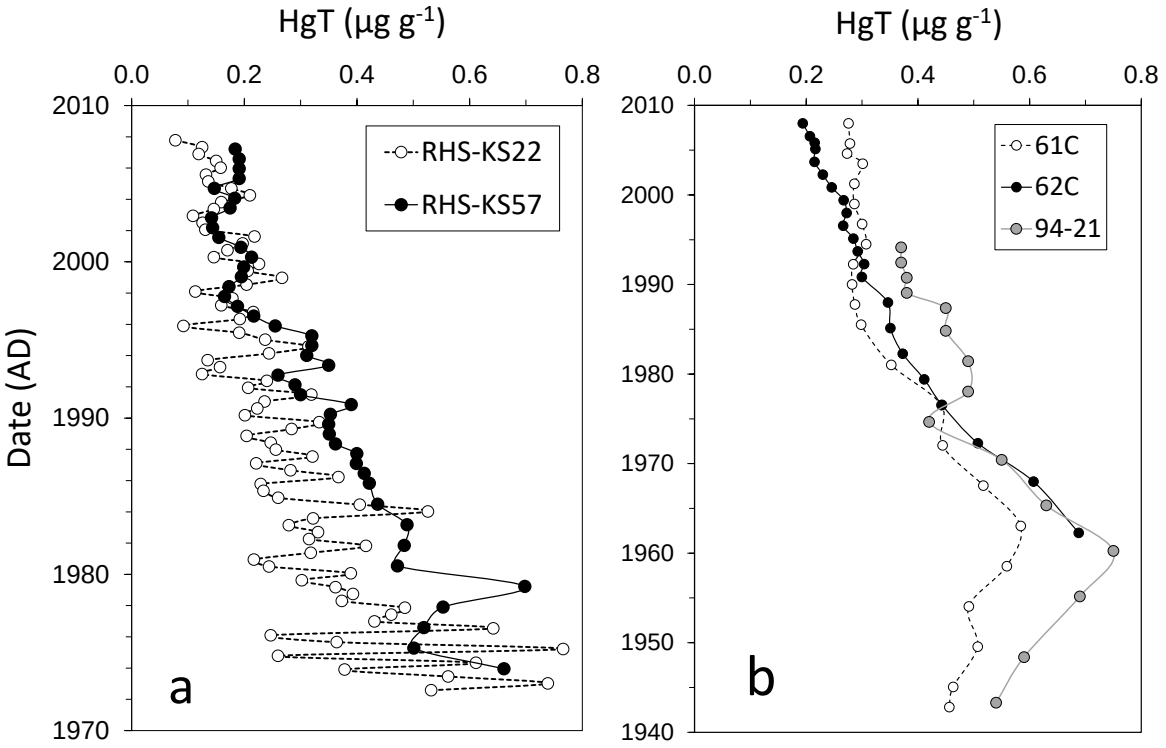
HgT (µg g-1)
0.0
0.2
0.4
0.6
0.8
2010
2000
1990
1980
1970
Date (AD)
RHS-KS22
RHS-KS57
a
HgT (µg g-1)
0.0
0.2
0.4
0.6
0.8
2010
2000
1990
1980
1970
1960
1950
1940
61C
62C
94-21
b

**Figure 3**.

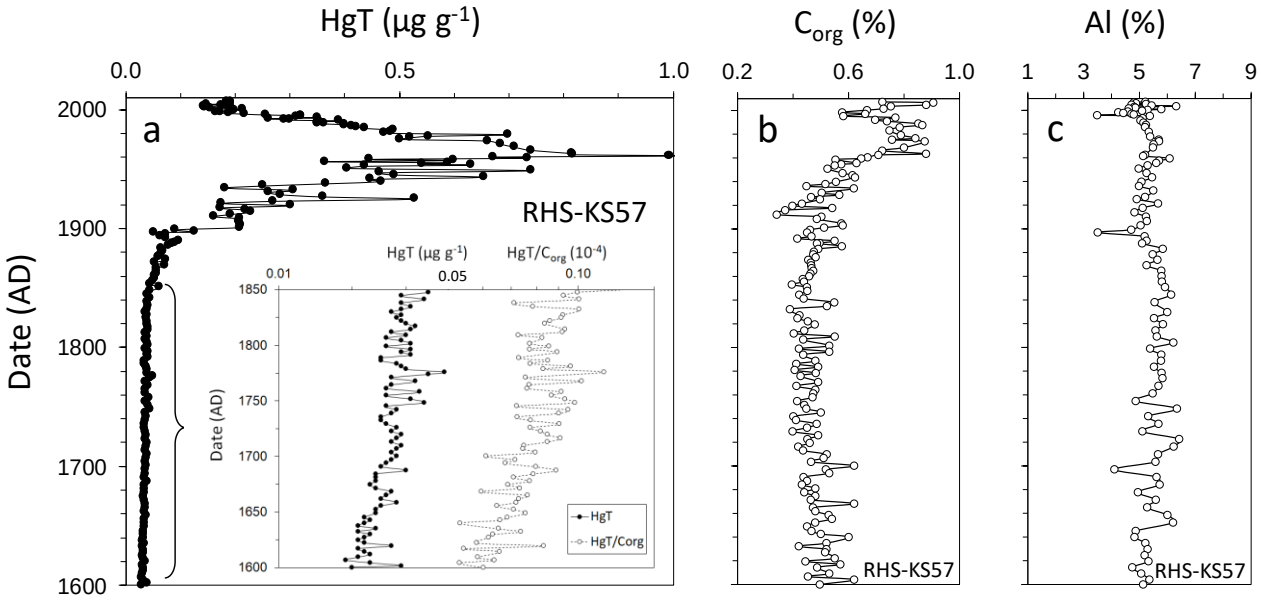


**Figure 4**.

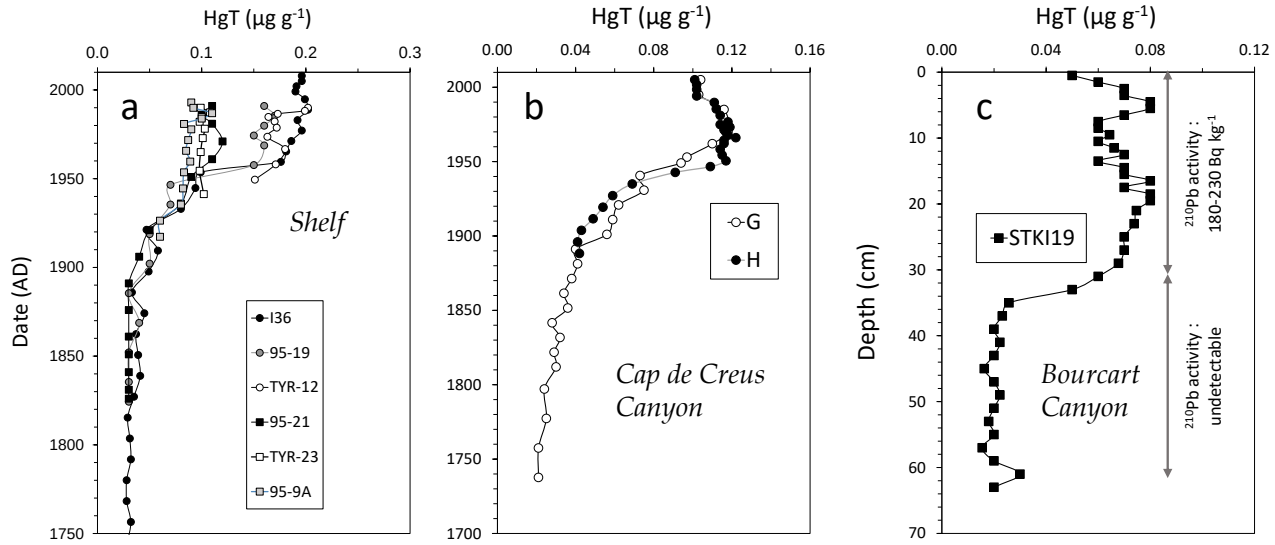


**Figure 5**.

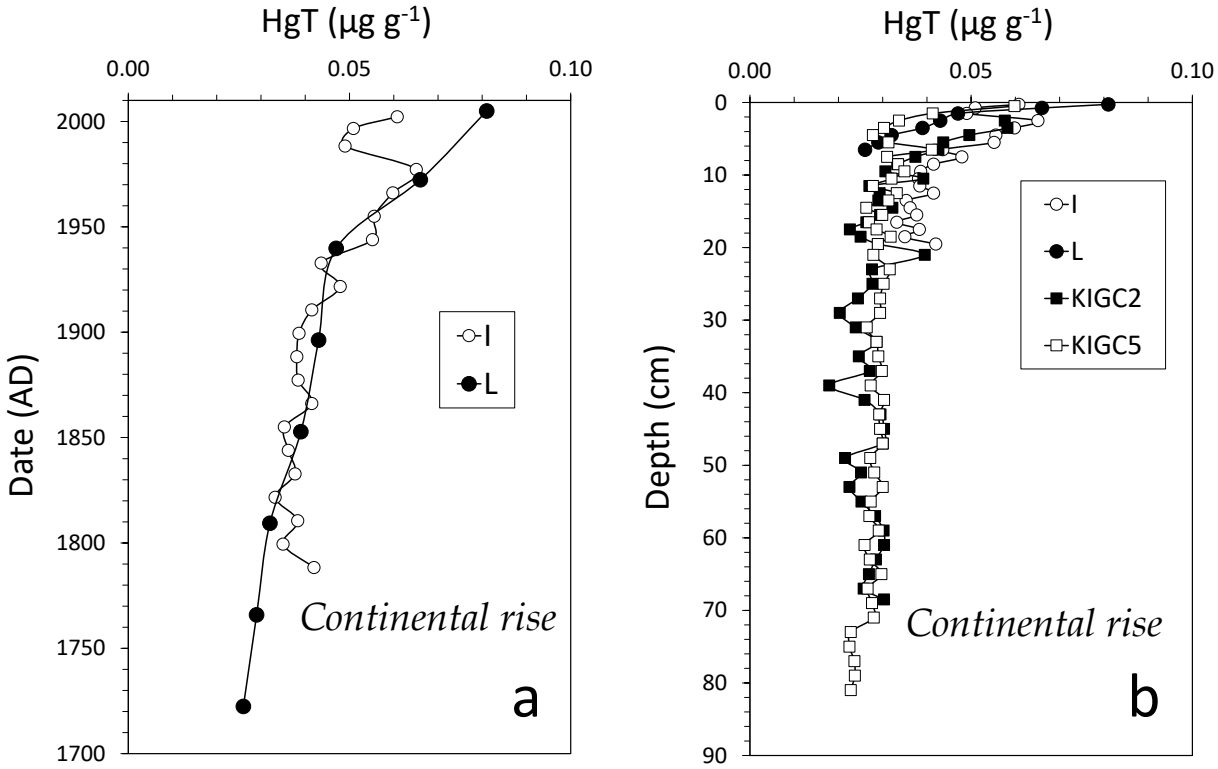
HgT (µg g-1)
0.00
0.05
0.10
2000
1950
1900
1850
1800
1750
1700
Date (AD)
I
L
Continental rise
a
HgT (µg g-1)
0.00
0.05
0.10
0
10
20
30
40
50
60
70
80
90
Depth (cm)
I
L
KIGC2
KIGC5
Continental rise
b

**Figure 6**.

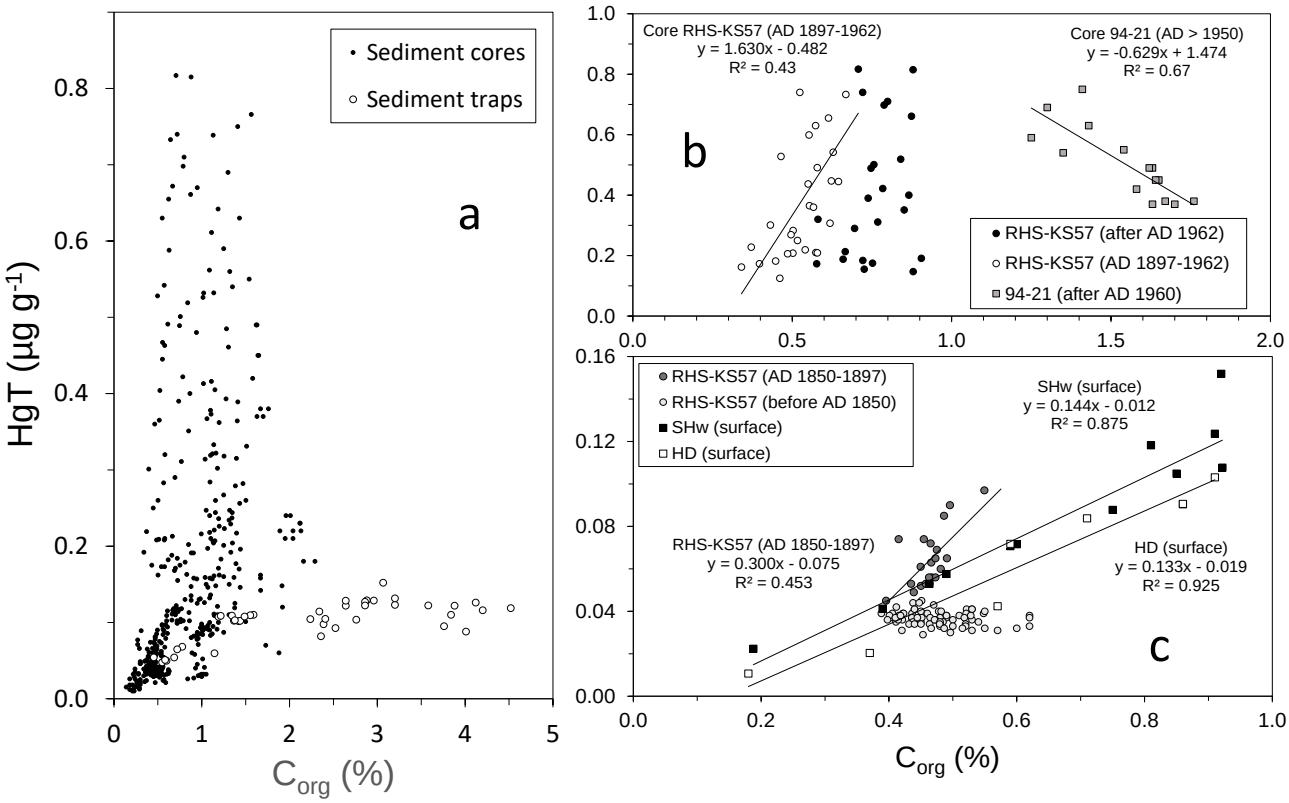
Sediment cores
Sediment traps
a
HgT (µg g-1)
Corg (%)
b
Core RHS-KS57 (AD 1897-1962)
y = 1.630x - 0.482
R² = 0.43
Core 94-21 (AD > 1950)
y = -0.629x + 1.474
R² = 0.67
RHS-KS57 (after AD 1962)
RHS-KS57 (AD 1897-1962)
94-21 (after AD 1960)
c
RHS-KS57 (AD 1850-1897)
RHS-KS57 (before AD 1850)
SHw (surface)
HD (surface)
SHw (surface)
y = 0.144x - 0.012
R² = 0.875
RHS-KS57 (AD 1850-1897)
y = 0.300x - 0.075
R² = 0.453
HD (surface)
y = 0.133x - 0.019
R² = 0.925
Corg (%)

**Figure 7**.

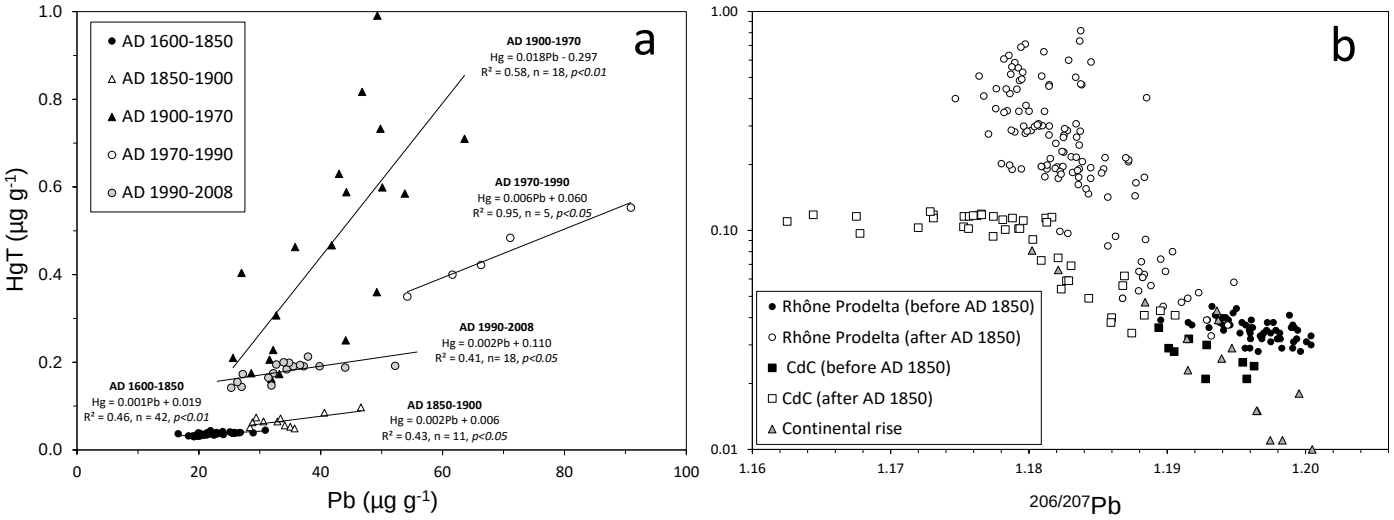
a
AD 1600-1850
AD 1850-1900
AD 1900-1970
AD 1970-1990
AD 1990-2008
AD 1900-1970
Hg = 0.018Pb - 0.297
R² = 0.58, n = 18, p<0.01
AD 1970-1990
Hg = 0.006Pb + 0.060
R² = 0.95, n = 5, p<0.05
AD 1990-2008
Hg = 0.002Pb + 0.110
R² = 0.41, n= 18, p<0.05
AD 1600-1850
Hg = 0.001Pb + 0.019
R² = 0.46, n = 42, p<0.01
AD 1850-1900
Hg = 0.002Pb + 0.006
R² = 0.43, n = 11, p<0.05
HgT (µg g-1)
Pb (µg g-1)
b
Rhône Prodelta (before AD 1850)
Rhône Prodelta (after AD 1850)
CdC (before AD 1850)
CdC (after AD 1850)
Continental rise
206/207Pb

**Figure 8**.

1170

# Sources, Transport, and Accumulation of Mercury in the Northwestern Mediterranean Margin Sediments during the Industrial Era

Cossa, D., R. Buscail, B. Dennielou, O. Radakovitch, P. Puig, A. Khripounoff, B. Boutier, S. Berné

## SUPPLEMENTARY INFORMATION

## Supplementary methods

### *SI.1. Sedimentation rates measurements for cores 95-19, 94-21, and 95-21.*

The geochronological study was performed using $^{210}$Pb and $^{137}$Cs. $^{210}$Pb is formed by the decay of $^{226}$Ra in sediment and of $^{222}$Ra in the water column and the atmosphere. The $^{210}$Pb formed by the second process is very rapidly associated with particles deposited as sediment, constituting the unsupported $^{210}$Pb used for dating purposes. If it is assumed that unsupported $^{210}$Pb concentration does not vary over time during the depositing of sediment, its law of exponential decay can be applied as a function of time to estimate the sedimentation rate for a given core sample. (Pheiffer Madsen and Sorensen, 1979).

If the sedimentation rate is constant and the sediment has not been disturbed, and if we do not take compaction into account, there is a linear relation between the depth Z of a given horizon and the age t of this horizon (the period between its deposit and removal): $Z = Kt$, where K is the sedimentation rate.

The decay of unsupported $^{210}$Pb follows an order of 1 kinetics. Thus, the activity A of the $^{210}$Pb in a given horizon during its burial is described by $dA = \lambda A\, dt$, where A is the activity of unsupported $^{210}$Pb and $\lambda$ its decay constant. The resolution of this equation gives $\ln A = \lambda t + C$. If it is assumed that the deposit has not been disturbed, the activity of unsupported $^{210}$Pb can be expressed by $\ln A = \lambda Z / K + C$. This equation can be transformed by replacing $\lambda$ with $T_{1/2}$ (half-life): $\lambda = \ln 2 / T_{1/2}$. Decimal logarithms are generally used so that the equation becomes:

$$log\ A = \frac{log\ 2 \times Z}{T_{1/2} \times K} + C' = R \times Z + C'\ R \times Z + C'$$

In any undisturbed layer of sediment to which this type of equation applies, or for which there is a significant linear regression between the depth of horizons in the sediment and the log of unsupported $^{210}$Pb activity, the sedimentation rate can be calculated: $K = \log 2 / (R \times T_{½})$, where R is the slope of the regression curve. $^{137}$Cs was introduced into the environment by man in 1952. Thus, the deepest horizon of a core sample containing $^{137}$Cs was at the surface of the sediment in 1952 sediment or, in the case of a bioturbated layer, at the base of this layer.

All elements required for the geochronological study were measured by gamma spectrometry at the Laboratory for Measurement of Environmental Radioactivity of the Institute for Protection and

Nuclear Safety (IPSN) in Orsay, France. $^{210}$Pb is characterized by gamma emission at 46.5 keV, bismuth-214 at 609.3 keV, lead-214 at 351.9 keV, and $^{137}$Cs at 661.7 keV. Unsupported $^{210}$Pb is determined by subtracting the mean amount of $^{214}$Bi and $^{214}$Pb from total $^{210}$Pb.

Reference: Pheiffer Madsen, P., Sørensen, J., 1979. Validation of the lead-210 dating method. J. Radioanal. Chem. 54, 39–48. Doi:10.1007/BF02517759

Core sample 94-21: This core, obtained on October 30, 1994, in the Rhône prodelta at a depth of 86 m, measured 31 cm and showed a uniform grain size, with more than 99 % of particles smaller than 63 µm. The upper layer between 0 and 4 cm was bio-mixed, as indicated by the vertical aspect of the log $^{210}$Pb/depth curve (Fig. A). Between 4 and 31 cm the activity of unsupported $^{210}$Pb decreased according to the equation:

$$\log {}^{210}\text{Pb} = -0.023\ Z + 2.322\ (R^2 = 0.93).$$

Based on this equation, the apparent sedimentation rate is:

$$0.30103 / (22.2 \times 0.023) = 0.59\ \text{cm a}^{-1}$$

In addition, $^{137}$Cs was detected down to 30 cm, which validates the calculation.

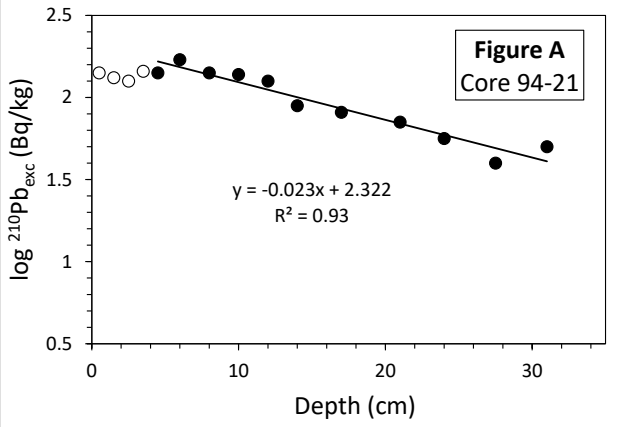


***Figure A**: $^{210}$Pb activity changes as a function of depth in the core 94-21*

Core sample 95-19: This 31-cm long core was obtained on October 25, 1995, at a depth of 73m and showed very uniform grain size (95 to 100% of particles smaller than 63 µm). The results for $^{210}$Pb showed two distinct zones of significant relationship: one between 0-8 cm, and the other between 11 and 31 cm. In between a drop in $^{210}$Pb activity suggests a layer of lower sedimentation (Fig. B).

Between 0 and 8 cm the linear relation between log $^{210}$Pb is:

$$\log {}^{210}\text{Pb} = -0.032\ Z + 2.176\ (R^2 = 0.87),\ \text{with a SR of } 0.42\ \text{cm a}^{-1}.$$

Between 11 and 31 cm the linear relation between log $^{210}$Pb is:

$$\log {}^{210}\text{Pb} = -0.033\ Z + 1.772\ (R^2 = 0.94),\ \text{with a SR of } 0.41\ \text{cm a}^{-1}.$$

In-between, there was a rapid decay of $^{210}$Pb between these two layers:

$$\log {}^{210}\text{Pb} = -0.123\ Z + 2.775\ (R^2 = 0.98)$$

which may correspond to a slower sedimentation episode with an SR of 0.11 cm a$^{-1}$.

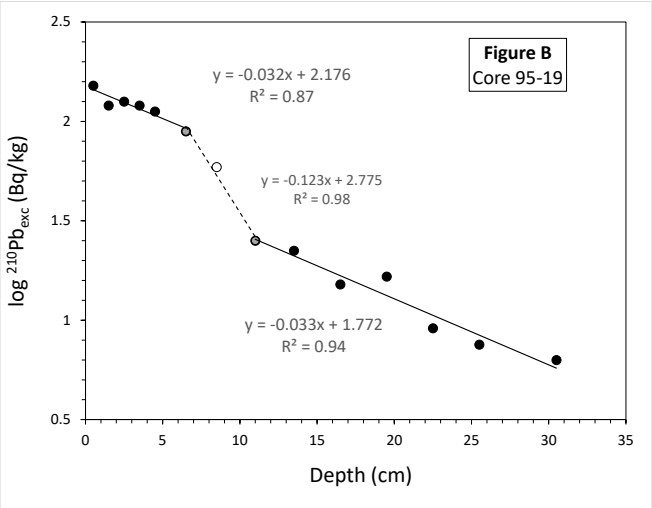


***Figure B:*** *$^{210}$Pb activity changes as a function of depth in the core 95–19*

61

62 Core sample 95-21: This core was obtained on October 28, 1995, at a depth of 50 m and consists of
63 fine sediment (96 to 99% of particles smaller than 63 µm). The $^{210}$Pb profile (figure 5a) displays a
64 linear decrease as a function of depth, according to the equation:

65 $$^{210}Pb = -0.0527\ Z + 2.090\ (R^2 = 0.92)$$

66 The sedimentation rate is deduced as follows: 0.30103 / (22.2 x 0.0527) = 0.26 cm/year.

67 This equation applies up to the superficial horizon, indicating that this core sample was undisturbed.

68 The last measurable $^{137}$Cs value was detected at 11.5 cm, which means that this horizon was at the surface
69 in AD 1952. As the $^{210}$Pb concentration suggests uniform sedimentation throughout the sample, the
70 sedimentation rate can be estimated from the $^{137}$Cs data. A burial of 11.5 cm in 43 years corresponds to
71 a sedimentation rate of 0.26 cm $a^{-1}$. This concordance between the two calculation methods tends to
72 validate the rate obtained.

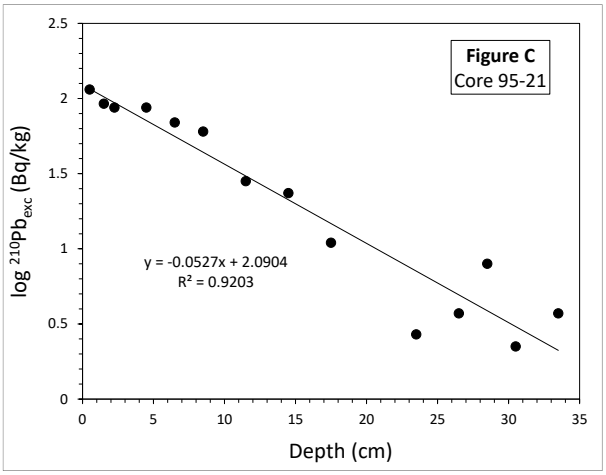


***Figure C:*** *Changes in $^{210}$Pb activities and metal concentrations as a function of year in the core 95–21*

73

74

## Supplementary Tables

***Table SI.1.*** *Sediment cores collected in the GoL: Site identification, location (Fig. 1), depth, date of collection, length of the core, and type of corer. (MC) Wuttke-type multicorer; (K) Kullenberg; (R) Reyneck box-corer. (BC) Bourcart Canyon; (CdC) Cap de Creus. Core lengths correspond to the sedimentary column analyzed, not the total length of the core. (*) Roustan lobe (proximal Rhône prodelta). RHS-KS22 : http://igsn.org/BFBGX-86649; RHS-KS57 : http://igsn.org/BFBGX-86607; STKI-19 : http://igsn.org/BFBGX-88837; KIGC-25 : http://igsn.org/BFBGX-87903; KIGC-02 : http://igsn.org/BFBGX-87942; KIGC-05 : http://igsn.org/BFBGX-87923.*

| Area | Station | Latitude (°North) | Longitude (°East) | Depth (m) | Core length (cm) | Corer | Sampling date (month/year) |
|---|---|---|---|---|---|---|---|
| Rhône prodelta* | ME | 43.3120 | 4.8483 | 18 | 32 | MC | 09/2011 |
| Rhône Prodelta* | RHS-KS22 | 43.3060 | 4.8497 | 43 | 835 | K | 09/2008 |
| Rhône Prodelta | 62C | 43.3022 | 4.9235 | 70 | 32 | MC | 09/2008 |
| Rhône Prodelta | RHS-KS57 | 43.2852 | 4.8495 | 79 | 767 | K | 09/2008 |
| Rhône Prodelta | 61C | 43.2317 | 4.8410 | 98 | 29 | MC | 09/2008 |
| Rhône Prodelta | 94-21 | 43.2500 | 4.8000 | 86 | 31 | R | 10/1994 |
| Shelf | I36 | 43.1957 | 4.5085 | 71 | 59 | MC | 09/2008 |
| Shelf | 95-19 | 43.2208 | 4.3667 | 73 | 32 | R | 10/1995 |
| Shelf | TYR12 | 43.2667 | 4.3167 | 63 | 35 | R | 11/1991 |
| Shelf | 95-21 | 43.3842 | 3.9983 | 58 | 34 | R | 10/1995 |
| Shelf | TYR23 | 43.2167 | 3.7833 | 81 | 35 | R | 11/1991 |
| Shelf | 95-9A | 42.9950 | 3.1061 | 25 | 28 | R | 10/1995 |
| BC Canyon | STKI19 | 42.7222 | 3.6961 | 478 | 63 | R | 04/2002 |
| CdC Canyon | G | 42.3078 | 3.6100 | 960 | 28 | MC | 10/2005 |
| CdC Canyon | H | 42.2253 | 3.8267 | 1473 | 34 | MC | 10/2005 |
| Continental slope | TYR20 | 42.5000 | 3.8333 | 750 | 12 | R | 11/1991 |
| Continental slope | KIGC25 | 42.6833 | 3.8525 | 341 | 72 | R | 10/2002 |
| Continental Rise | I | 42.2147 | 4.2556 | 1874 | 20 | MC | 10/2005 |
| Continental Rise | L | 42.0783 | 4.6667 | 2335 | 8 | MC | 10/2005 |
| Continental Rise | KIGC2 | 41.9298 | 4.7193 | 2411 | 69 | K | 10/2002 |
| Continental Rise | KIGC5 | 41.9732 | 4.6952 | 2395 | 82 | K | 10/2002 |

***Table SI.2**. Sediment traps. Mooring sites, water depth, and dates of collection. Station HD: Settling particles were collected from October 2004 to May 2005, a period of major cascading and storm events in the GoL (Puig et al., 2008; Tesi et al., 2010), using a sediment trap (PPS3, Technicap®) placed at 30 m above the bottom at the CdC Canyon head (Fig. 1). Stations I and L: Settling particles were collected from April 2008 to July 2008, using a sediment trap (PPS5, Technicap®) placed at 20 m above the bottom of the continental rise (I and L, Fig. 1).*

| Station | Latitude (°North) | Longitude (°East) | Water depth (m) | Technicap® trap (collecting area) | Beginning of sampling | End of sampling |
|---|---|---|---|---|---|---|
| HD | 42.3712 | 3.3615 | 500 | PPS3 (0.125 $m^2$) | 29 Sept. 2004 | 18 May 2005 |
| I | 42.2500 | 4.3460 | 2113 | PPS5 (1 $m^2$) | 28 March 2008 | 6 June 2008 |
| L | 42.1667 | 4.5500 | 2226 | PPS5 (1 $m^2$) | 4 April 2008 | 4 July 2008 |

***Table SI.3.** Sedimentation rates (SR) with references and periods covered by the core. (*) SR deduced from the previous determinations in close vicinity (Touzani and Giresse, 2002; Charmasson et al., 2008 Beaudouin et al., 2005; Charmasson et al., 2008); (**) SR value from the value calculated for Core KTR05 collected at 200 m northward (Beaudouin et al., 2005). No SR is available for cores I36, KIGC2, 5, and 25, STKI19, and TYR20.*

*Beaudouin, C., Suc, J.-P., Cambon, G., Touzali, A., Giresse, P., Pont, D., Aloïsi, J.-C., Marsset, T., Cochonat, P., Duzer, D., Ferrier, J., 2005. Present-day rhythmic deposition in the Grand Rhone prodelta (NW Mediterranean) according to high-resolution pollen analyses. J. Cstl. Res. 21 (2), 292-306. https://www.jstor.org/stable/4299416*

*Charmasson S., Radakovitch O., Arnaud M., Bouisset P., Pruchon A.S., 1998. Long-core profiles of $^{137}Cs$, $^{134}Cs$, $^{60}Co$, and $^{210}Pb$ in sediment near the Rhône River (Northwestern Mediterranean Sea). Estuaries 21, 367–378. Doi:10.2307/1352836.*

*Cossa, D., Buscail, R., Puig, P., Chiffoleau, J.-F., Radakovitch, O., Jeanty, G., Heussner, S., 2014a. Origin and accumulation of trace elements in sediments of the northwestern Mediterranean margin. Chem. Geol. 380, 61-73. Doi:10.1016/j.chemgeo.2014.04.015*

*Fanget, S., Bassetti, M.-A., Arnaud, M. Chiffoleau, J.-F., Cossa, D., Goineau, A., Fontanier, C., Buscail, R., Jouet, G., Maillet, G.M., Negri, A., Dennielou, B., Berné, S., 2013. Historical evolution and extreme climate events during the last 400 years on the Rhone prodelta (NW Mediterranean). Mar. Geol. 346, 375-391. Doi: 10.1016/j.margeo.2012.02.007*

*Fanget, A.-S., Berné, S., Jouet, G., Bassetti, M.-A., Dennielou, B., Maillet, G. M., Tondut, M., 2014. Impact of relative sea level and rapid climate changes on the architecture and lithofacies of the Holocene Rhône subaqueous delta (Western Mediterranean Sea). Sediment. Geol. 305, 35–53. Doi:10.1016/j.sedgeo.2014.02.004*

*RNO. 1998. Surveillance du Milieu Marin. Travaux du RNO. Edition 1998. Ifremer et Ministère de l'Aménagement du Territoire et de l'Environnement. https://archimer.ifremer/doc/00314/42561 http://envlit.ifremer.fr/content/download/27652/224839/version/2/file/rno98.pdf*

*Touzani, A., Giresse, P., 2002. The Rhône River Prodelta: Short-Term ($10^0$-$10^3$ Year) Sedimentation Patterns and Human Impact. J. Cstl. Res. 18 (1), 102-117.*

*Zuo, Z., Eisma, D., Gielest, R., Beks, J., 1997. Accumulation rates and sediment deposition in the northwestern Mediterranean. Deep-Sea Res. Part II 44 (34), 591409. Doi:10.1016/S0967-0645(96)00083-5*

| Core | SR (cm $a^{-1}$) | Period (AD) | Reference |
|---|---|---|---|
| ME | >20 | 2011 – 2010 | * |
| RHS-KS22 | 17** | 2008 – 1953 | Beaudouin et al. (2005) |
| RHS-KS57 | Depend on the periods | 2008 – 1600 | Fanget et al. (2013, 2014) |
| 61C | 0.45 ± 0.05 | 2008 – 1943 | * |
| 62C | 0.70 ± 0.05 | 2008 – 1962 | * |
| 94-21 | 0.59 | 1993 – 1943 | Suppl. Info. SI.1 |
| 95-19 | 0.42 / 0.11 / 0.41 | 1991 – 1900 | Suppl. Info. SI.1 |
| TYR12 | 0.36 ± 0.04 | 1990 – 1958 | Zuo et al. (1997) |
| 95-21 | 0.26 | 1991 -1870 | Suppl. Info. SI.1 |
| TYR23 | 0.10 ± 0.01 | 1990 – 1942 | Zuo et al. (1997) |
| 95-9A | 0.33 ± 0.10 | 1993 -1918 | RNO (1998) |
| G | 0.19 ± 0.02 | 2005 – 1710 | Cossa et al. (2014a) |
| H | 0.18 – 0.52 | 2005 – 1850 | Cossa et al. (2014a) |
| I | 0.06 | 2005 – 1780 | Cossa et al. (2014a) |
| L | 0.02 | 2005 – 1720 | Cossa et al. (2014a) |

***Table SI.4****. Basis for the calculation of the anthropogenic Hg accumulated in the GoL sediments. Proximal prodelta area is defined by an envelope of 3 km on either side of the mouth of the Rhône River between the isobaths 10 and 40 m, the distal part by an envelope between 40 and 100m. The Hg inventories are calculated as* $\sum_{k=0}^{n} \binom{n}{k} \rho\ [Hg\text{anthr}]\ V\ (1-\beta)$

*with ρ the density, β the porosity, V the volume of the layer, and [$Hg_{anthr}$] the concentration of the anthropogenic Hg in the layer (i.e., Hg measured minus Hg background), n being the number of layers in the core. The pre-industrial Hg concentrations are the HgT concentrations at the bottom of the core, i.e., sediments deposited before AD 1850.*

| Zone | Surface area ($km^2$) | $Hg_{anthr}$ inventory (μg $cm^2$) | Pre-industrial Hg (μg $g^{-1}$) |
|---|---|---|---|
| Proximal prodelta | 10 | 320 | 0.035 |
| Distal prodelta | 20 | 166 | 0.030 |
| Inner shelf | 1000 | 1-2.5 | 0.035 |
| Outer shelf | 3000 | 0.2-1 | 0.030 |
| CdC Canyon | 40 | 1.6 | 0.025 |
| Continental rise | $10^4$ | 0.2 | 0.013 |

## Supplementary figures

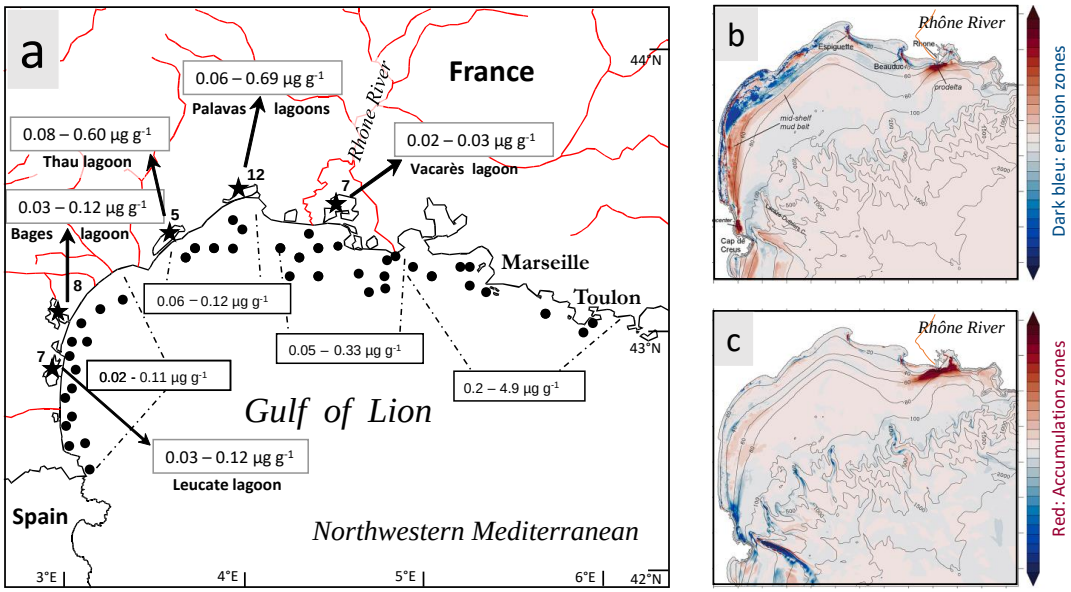


***Figure SI.1***. *(a) Hg concentration ranges in the < 63µm fraction of the surface sediments of the inner shelf of the Gulf of Lion and coastal lagoons (source: https://littoral.ifremer.fr/Reseaux-de-surveillance/Environnement/ROCCH-Reseau-d-Observation-de-la-Contamination-CHimique-du-littoral); (b) and (c) thickness of the deposition in autumns and winters 2010-11 and 2010-12, respectively, adapted from Estournel et al. (2023).*

*Estournel, C., Mikolajczak, G., Ulses, C., Bourrin, F., Canals, M., Charmasson, S., Doxaran, D., Duhaut, T., Durrieu de Madron, X., Marsaleix, P., Palanques, A., Puig, P., Radakovitch, O., Sanchez-Vidal, A., Verney, R., 2023. Sediment dynamics in the Gulf of Lion (NW Mediterranean Sea) during two autumn-winter periods with contrasting meteorological conditions. Progr. Oceanogr. 210, 102042. Doi:10.1016/j.pocean.2022.102942*

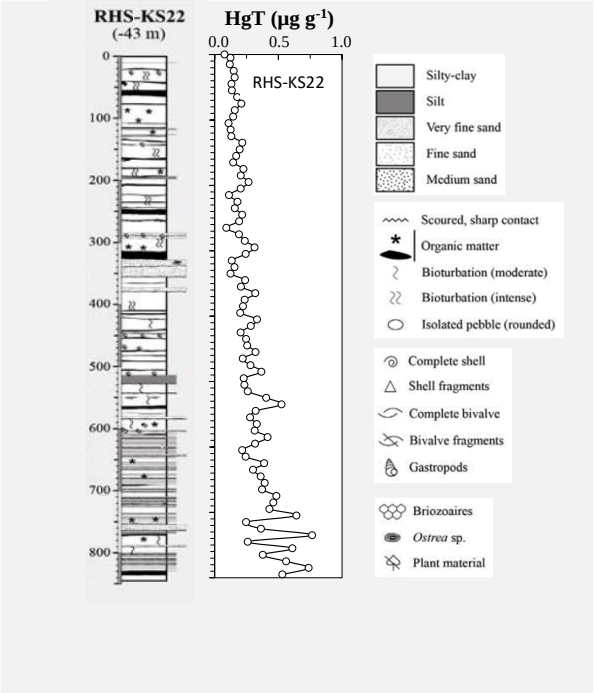


***Figure SI.2****. HgT profile (this work) and lithologic description of Core RHS-KS22 adapted from Fanget et al. (2014).*

*Fanget, A.-S., Berné, S., Jouet, G., Bassetti, M.-A., Dennielou, B., Maillet, G.M., Tondut, M., 2014. Impact of relative sea level and rapid climate changes on the architecture and lithofacies of the Holocene Rhone subaqueous delta (Western Mediterranean Sea). Sediment. Geol. 305, 35–53. Doi:10.1016/j.sedgeo.2014.02.004*

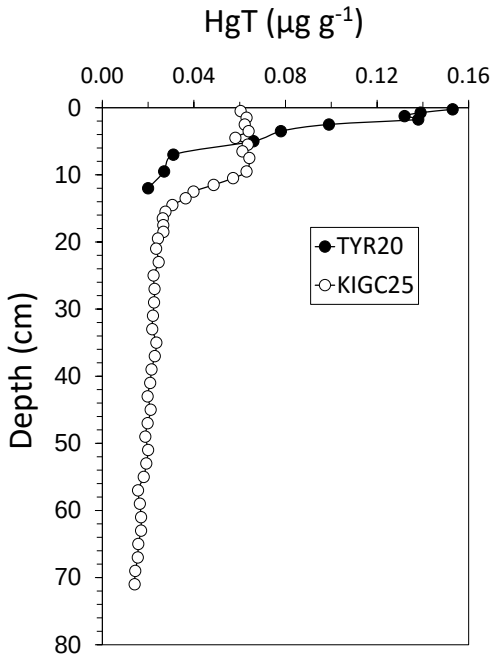


***Figure SI.3****. Mercury concentration profile (HgT)* versus *depth in sediment cores from the interfluves (TYR20 and KIGC25).*

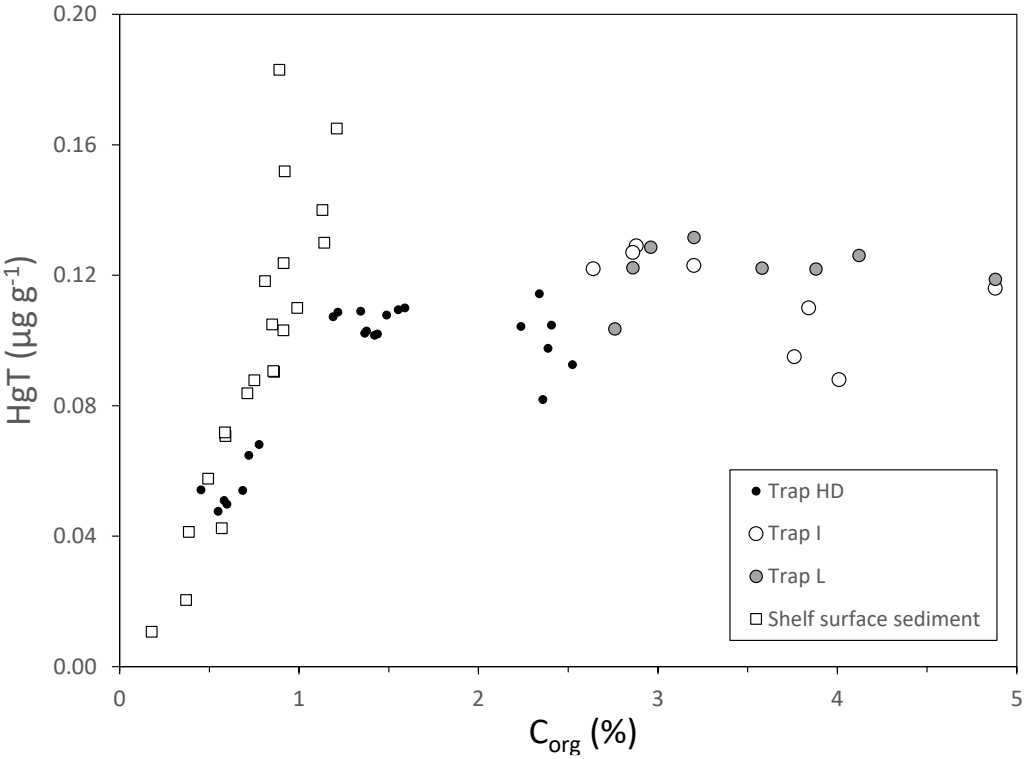


***Figure SI.4***. *Mercury (HgT)* versus *organic carbon ($C_{org}$) in the trap material and surface sediment from the Gulf of Lion shelf.*

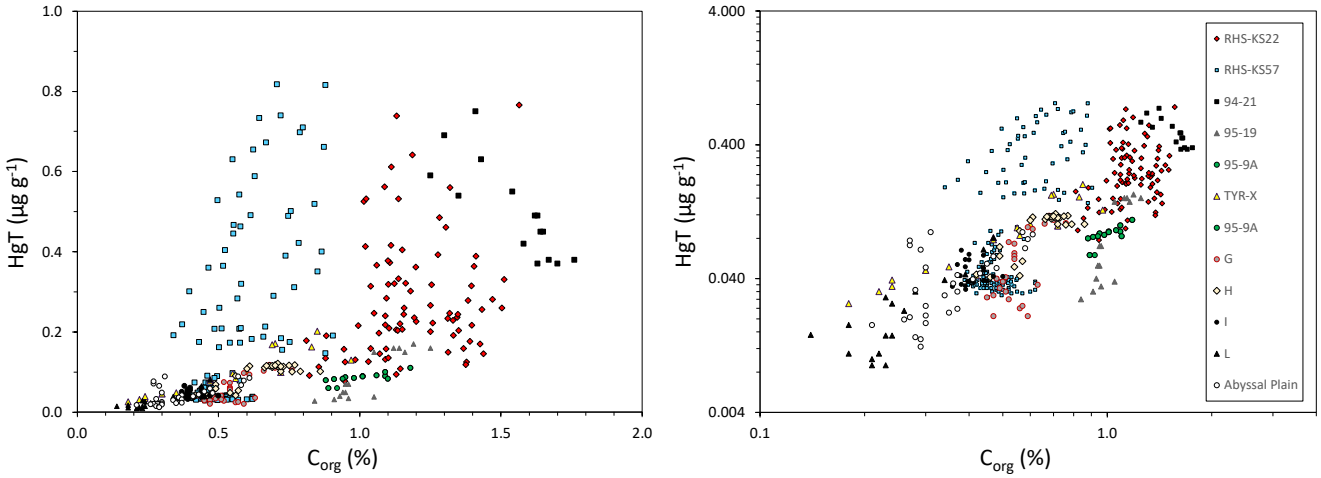


***Figure SI.5***. *Mercury (HgT)* versus *organic carbon ($C_{org}$) in sediment cores from the Gulf of Lion.*

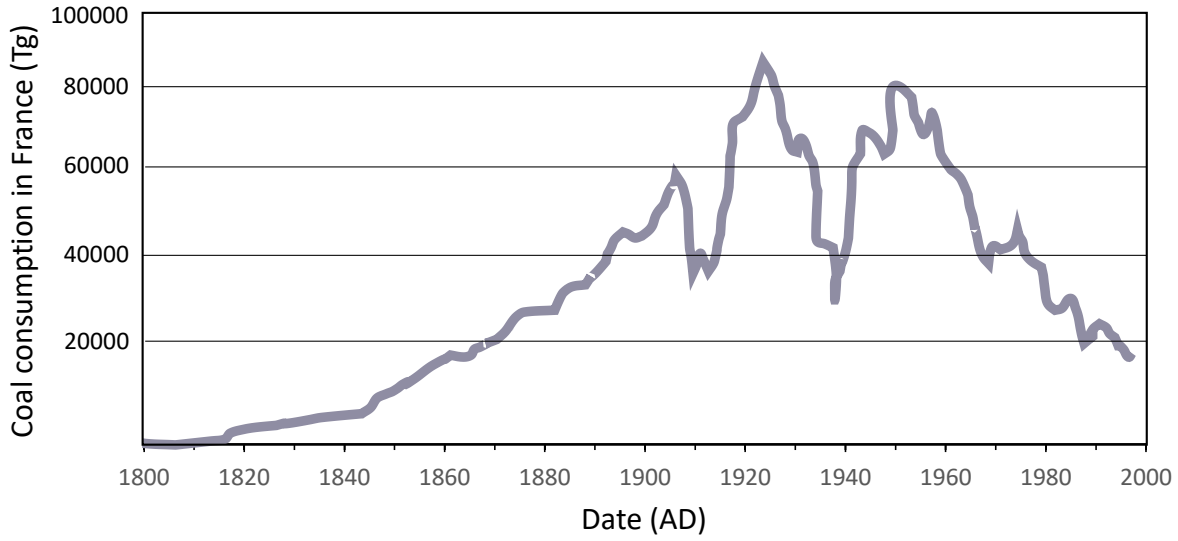


***Figure SI.6****. Coal consumption in France between AD 1787 and AD 1997. Adapted from Conus, M.-F., and J.-L. Escudier. 2006. Cycle de vie et relation capital/travail : Application à l'industrie houillère française 1720-2004. In :* Territoires européens du charbon des origines aux reconversions. *p.53-73; Daumalin, X., Daviet, S., and Mioche P. editors. Presses universitaires de Provence, Aix-en-Provence, France; pp. 282. Doi:10.4000/books.pup.624*

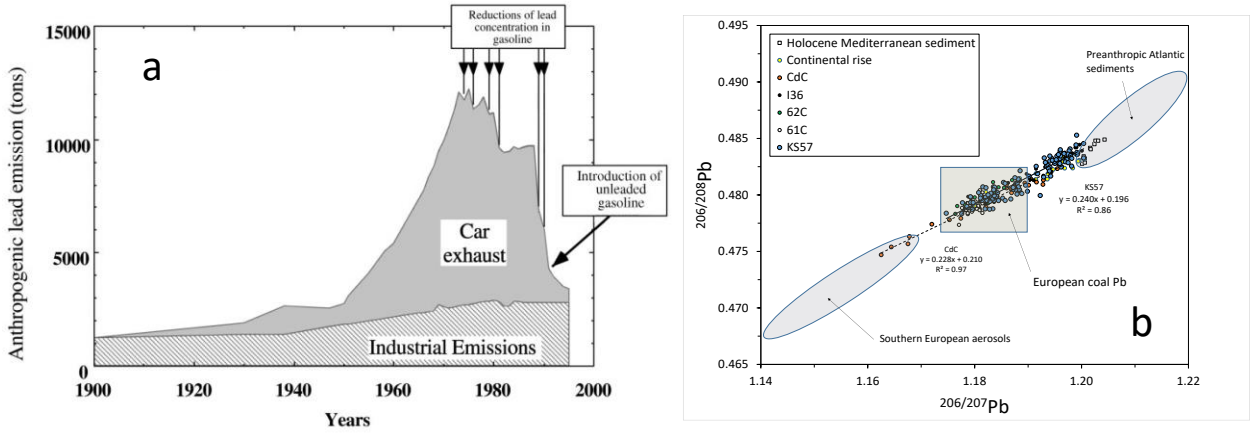


***Figure SI.7****. (a) Anthropogenic lead emissions in France between AD 1900 and 2000 (adapted from Ferrand et al., 1999); (b) Isotopic composition of various sediment cores in the GoL (adapted from Cossa et al., 2014a, 2018a).*

*Ferrand, E., Eyrolle, F., Radakovitch, O., Provansal, M., Dufour, S., Vella, C., Raccasi, G., Gurriaran, R., 2012. Historical levels of heavy metals and artificial radionuclides reconstructed from overbank sediment records in lower Rhône River (South-East France). Geochim. Cosmochim. Acta 82, 163-182. Doi:10.1016/j.gca.2011.11.023*

*Cossa, D., Buscail, R., Puig, P., Chiffoleau, J.-F., Radakovitch, O., Jeanty, G., Heussner, S., 2014 Origin and accumulation of trace elements in sediments of the northwestern Mediterranean margin. Chem. Geol. 380, 61-73. Doi:10.1016/j.chemgeo.2014.04.015*

*Cossa, D., Fanget, A.-S., Chiffoleau, J.-F., Bassetti, M.-A., Buscail, R., Deninelou, B., Briggs, K., Arnaud, M., Guédron, S., Berné, S., 2018a. Chronology and sources of trace elements accumulation in the Rhône pro-delta sediments (Northwestern Mediterranean) during the last 400 years. Progr. Oceanogr. 163, 161-171. Doi:10.1016/j.pocean.2017.01.008*

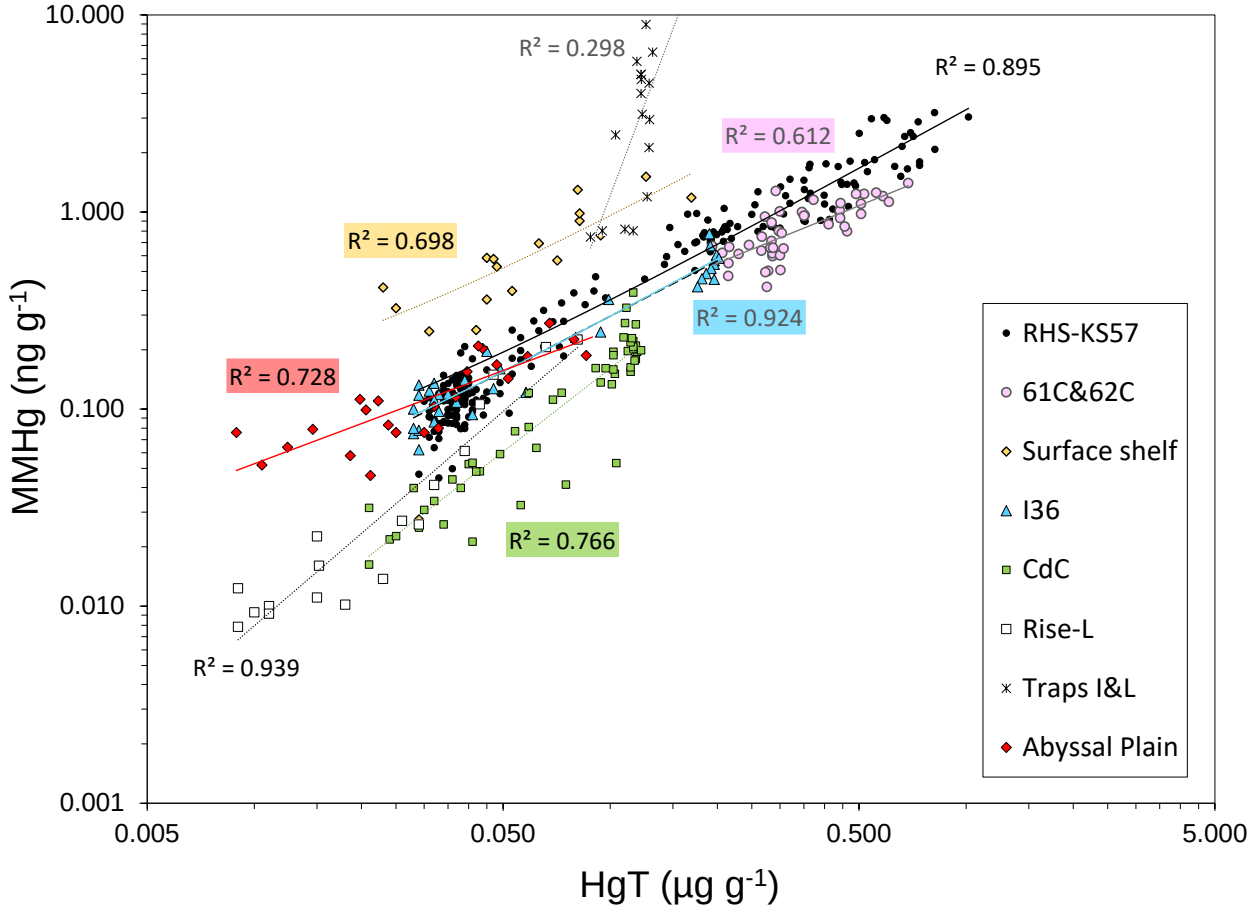


***Figure SI.8***. *Monomethyl mercury (MMHg)* versus *total Hg (HgT) in sediments of the Gulf of Lion and adjacent marine areas (see Fig. 1 in the manuscript). CdC: Cap de Creus Canyon. Abyssal plain of the Western Mediterranean (adapted from Cossa et al., 2021).*

*Cossa, D., Mucci, A., Guédron, S., Coquery, M., Radakovitch, O., Escoube, R., Campillo, S. Heussner, S., 2021. Mercury accumulation in the sediment of the Western Mediterranean abyssal plain: A reliable archive of the late Holocene. Geochim. Cosmochim. Acta 309, 1-15. Doi:10.1016/j.gca.2021.06.014*

## Electronic Supplementary

See: EXCEL file "*Data_Hg_GoL_(Cossa et al., 2023)*"